Bioactive Materials 6 (2021) 26–44

Contents lists available at ScienceDirect

Bioactive Materials

journal homepage: http://www.keaipublishing.com/biomat

# Structural and mechanical aspects of hypoeutectic Zn–Mg binary alloys for biodegradable vascular stent applications

W. Pachla[a,*,1], S. Przybysz[a], A. Jarzębska[b], M. Bieda[b], K. Sztwiertnia[b], M. Kulczyk[a], J. Skiba[a]

[a] Institute of High Pressure Physics, Polish Academy of Sciences UNIPRESS, Warszawa, Poland
[b] Institute of Metallurgy and Materials Science, Polish Academy of Sciences, Krakow, Poland

ARTICLE INFO

*Keywords:*
Biodegradable Zn alloys
Hydrostatic extrusion
Microstructure
Mechanical properties
Vascular stent

ABSTRACT

The study is concerned with the mechanical properties of Zn and three Zn–Mg double alloys with Mg concentrations: 0.5%, 1.0% and 1.5% in the form of rods with a diameter of 5 mm as potential materials for use in biodegradable medical implants, such as vascular stents. The materials were cast, next conventionally hot extruded at 250 °C and finally, hydrostatically extruded (HE) at ambient temperature. Occasionally HE process was carried at liquid nitrogen temperature or in combination with the ECAP process. After HE, the microstructure of the alloys was made up of fine-grained αZn of mean grain size ~1 μm in a 2-phase coat of 50–200 nm nanograins of the fine αZn + $Mg_2Zn_{11}$ eutectic. The 3 to 4-fold reduction of grain size as a result of HE allowed an increase in yield strength from 100% to over 200%, elongation to fracture from 100% to thirty fold and hardness over 50% compared to the best literature results for similar alloys. Exceptions accounted for elongation to fracture in case of Zn-0.5 Mg alloy and hardness in case of Zn-1.5 Mg alloy, both of which fell by 20%. For the Zn-0.5 Mg and Zn–1Mg alloys, after immersion tests, no corrosive degradation of plasticity was observed. Achieving these properties was the result of generating large plastic deformations at ambient temperature due to the application of high pressure forming with the cumulative HE method. The results showed that Zn–Mg binary alloys after HE have mechanical and corrosive characteristics, qualifying them for applications in biodegradable implants, including vascular stents.

## 1. Introduction

Zn–Mg binary alloys are a reasonable alternative to Mg alloys for implantology applications. Earlier researches on biodegradable materials focused their attention mainly on magnesium or iron as well as on their alloys [1]. However very crucial feature of these materials is not optimal. Magnesium corrodes too quickly in the human body – it is resorbed before the healing of damaged tissue. In turn, the iron has a low corrosion rate and, consequently, is in contact with the tissue much longer than necessary. This creates the potential offered by Mg-doped Zn, demonstrating improved resistance to corrosion degradation and mechanical properties [2,3]. The microstructure of Zn–Mg binary alloys obtained by melting at 500 °C in open air shows large, equiaxial grains of pure Zn of medium size ~500 μm and the eutectic mixture of Zn + $Mg_2Zn_{11}$ [4]. For the Zn–1Mg alloy, after additional forming, the yield strength YS increased more than 2-fold to ~230 MPa, while higher casting alloys > 1.5% Mg cracked before the start of plastic flow without reaching yield strength. The yield strength of the Zn–1Mg alloy is a result of microstructure refinement and homogeneous distribution of the hard and brittle intermetallic phase of $Mg_2Zn_{11}$. Whereas total alloy brittleness ~3% Mg is attributed to the formation of large, 500 μm areas of the structure with a different spatial orientation after casting, which increases the hardness of the alloys to over 200 HV but dramatically decreases the UTS strength below 30 MPa and plasticity to $\varepsilon_f$ ~0.2% [4]. Such alloys become completely brittle and are not suitable for further forming by conventional methods. This is the result of eutectic domination of the structure, which according to the phase diagram for the Zn–Mg system contains approximately 3.5% Mg.

Therefore, for Zn–Mg binary alloys it becomes necessary to additionally increase the mechanical properties of Zn–Mg casting alloys, which has been attempted, although with moderate results, in many publications through a combination of plastic deformation with heat

Peer review under responsibility of KeAi Communications Co., Ltd.
* Corresponding author.
*E-mail addresses:* wacek@unipress.waw.pl (W. Pachla), sylwia@unipress.waw.pl (S. Przybysz), a.jarzebska@imim.pl (A. Jarzębska), m.bieda@imim.pl (M. Bieda), k.sztwiertnia@imim.pl (K. Sztwiertnia), mariusz@unipress.waw.pl (M. Kulczyk), skiba@unipress.waw.pl (J. Skiba).
[1] www.hydroextrusion.pl.

https://doi.org/10.1016/j.bioactmat.2020.07.004
Received 27 May 2020; Received in revised form 1 July 2020; Accepted 7 July 2020

treatment [4–7]. Therefore, the authors of this paper proposed a more effective way of increasing the properties of Zn–Mg binary alloys by pre-forming the casting material combined with another severe plastic deformation (SPD) obtained by cold cumulative hydrostatic extrusion (HE). This approach is supported by widely confirmed facts that biodegradable metals, due to their mechanical properties, are more useful for heavily loaded, biodegradable implants than polymeric materials [8,9].

Vojtech et al. [10] studied the mechanical properties and in vitro biodegradation of cast Zn–Mg binary alloys in the range of Mg content from 0.5 to 3 wt%. They found that the corrosion rate for Zn–Mg binary alloys, while not changing significantly with the percentage of Mg, is much lower compared to Mg alloys. Their strength and elongation reached 190 MPa and 1.8% at 1% Mg and decreased above this value. As they assumed, this was due to an excessive amount of brittle eutectic phase. Such low elongation is insufficient for many applications of biodegradable implants. In addition, Zn–Mg castings are characterised by a natural tendency to create a heterogeneous microstructure, which favours heterogeneous corrosion in places including fast corroded Mg. Therefore, taking into account the mechanical properties, homogeneity of biodegradation and cytotoxicity typical of most Zn–Mg binary alloys intended as an initial material for biodegradable implants, a combination of cast material with subsequent forming has been sought as a solution in recent years. Several papers on biodegradable Zn–Mg binary alloys have been published in last two years concerning second phases and their significant influences on alloy properties [11], inhibition of twinning by the refined $Mg_2Zn_{11}$ intermetallic phase [12], ultra-low concentration of Mg 0.08 wt% as the alloying element for potential biodegradable material for stent applications [13], contribution of work hardening, dynamic recrystallisation softening and grain boundary strengthening in the mechanical properties evolution, changing in a wide range of strength and elongation [14], Zn–Mg binary alloys as a suitable solution for medical or industrial applications of degradable materials that provide corrosion degradation periods ranging from those given by magnesium alloys and those derived from iron-based alloys [15,16] and the design and synthesis of microalloying Zn–Mg biodegradable metals with improved mechanical properties, which relies on the synergetic effects of both grain refinement and fast cooling [17]. A comprehensive review by Venezuela and Dargusch [18] summarizes the influence of alloying and fabrication techniques on the mechanical properties, biodegradability and biocompatibility of zinc and zinc alloys.

In the process of casting Zn–Mg binary alloys, different intermetallic phases are formed in their microstructure, depending on composition, melting and crystallisation conditions [11,19]. These various phases differ in brittleness, hardness and toughness [9]. Their uneven distribution may lead to differences in mechanical and degradation properties in the microstructure of the cast alloy. Additionally, the casting process usually generates defects, such as porosity and gas entrapment, which additionally influence the alloy's behaviour [20]. Heat treatment, such as homogenisation of alloys after casting, is the simplest and most commonly used method for Zn–Mg binary alloys to eliminate or reduce these defects [21]. This method, however, reduces the properties, especially the strength properties of these alloys. Therefore, for Zn–Mg binary alloys intended, among others, for biodegradable vascular stents, it is necessary to look for another way related to cold forming, which is the subject of this paper.

## 2. Materials and methods

### 2.1. Initial materials and methods

The materials used in the experiments were zinc alloys with 0.5, 1.0 and 1.5 wt% of magnesium, hereinafter designated as Zn-0.5 Mg, Zn–1Mg and Zn-1.5 Mg. Pure zinc determined as Zn was tested as a reference material. The alloys were prepared by gravity casting to steel mold of melted Zn or Zn and Mg (each element purity was 99.99%) in Naberthem N20/14 resistance furnace at temperature 650 °C under argon atmosphere. The as-cast ingots with a diameter of 75 mm were obtained. After turning the top layer, castings with a diameter of ~72 mm were conventionally hot extruded at 250 °C as rods with a diameter of 30 mm, i.e. with a reduction of R = 5.76, where R is the ratio of the rod cross-section before and after extrusion. This corresponds to the true strain $\varepsilon = 1.75$, where the true strain means the natural logarithm of reduction $\varepsilon = \ln R$.

The microstructure was examined on longitudinal rod cross-sections using transmission electron microscopy TEM (FEI TECNAI G2 F20), optical microscopy LM (Nikon Eclipse LV150) and scanning electron microscopy SEM (Hitachi TM-3000). Samples for LM and SEM were ground and polished. TEM films were prepared according to standard, commonly used procedures. The microstructure was evaluated on the basis of an average grain size calculated from maps of 50 × 50 $\mu m^2$ using the FEI Quanta 3D FEG scanning electron microscope equipped with the EDAX OIM TSL EBSD data collection system. The observation was carried out on longitudinal and transverse sections against the direction of the extruded rod. Grain size $d_{eq}$ was estimated on the basis of the diameter of the circle equivalent to the measured area and the grain size distribution.

The mechanical properties included hardness tests, static tensile tests and static uni-axial compression tests. Microhardness was measured on transverse and longitudinal rod cross-sections using the Zwick-Roell ZHV1-A automated microhardness tester at a load of 200 g during 15 s. The static fracture and uni-axial compression tests were conducted on a static Zwick/Roell Z250 kN universal testing machine at room temperature. Static fracture samples with a diameter of 3 mm and a length/diameter ratio of 5:1 were tested at a constant tensile rate of 0.008 $s^{-1}$, while compression samples with a diameter of 5 mm and a height/diameter ratio of 1.5:1 were compressed to 80% compression strain at a compression rate of 5 MPa $s^{-1}$.

Corrosion, more precisely in vitro degradation, was examined using immersion test carried out in simulated body fluids in Hanks' solution under conditions imitating conditions in human body (temperature = 37 °C, pH = 7.4). Samples cut off from the hydrostatically extruded rods of 5 mm in diameter and ~10 mm in height were kept in Hanks' solution under controlled condition up to 6 months. After period of times 1 week, 2 weeks, 1.5 month, 3 months, 4.5 months and 6 months weight loss and Vickers microhardness HV0.2 at the tranverse sections of immersed samples were measured. After hardness measurements, static uni-axial compression tests to evaluate compressive yield strength $\sigma_{0.2}$ were carried out, with this same process parameters as it was mentioned in previous paragraph.

### 2.2. Structure and mechanical properties after hot extrusion

After hot extrusion, the structure of rods consisted of αZn grains and the eutectic composed of αZn and the intermetallic phase of $Mg_2Zn_{11}$ distributed along the grain boundaries, Fig. 1. Occasionally, black areas corresponding to the intermetallic phase of $Mg_2Zn_{11}$ were observed. Of course, the share of eutectic increased as the share of Mg added to the alloy increased. The grain size decreased with Mg volume and was 220 μm for Zn and 48 μm, 33 μm and 16 μm for Zn-0.5 Mg, Zn–1Mg and Zn-1.5 Mg alloys, respectively. The mechanical properties of rods after casting were, respectively, for Zn-0.5 Mg, Zn–1Mg and Zn-1.5 Mg: ultimate tensile strength (UTS) 190 MPa, 310 MPa and 345 MPa, yield strength (YS) 150 MPa, 225 MPa and 275 MPa, elongation to fracture ($\varepsilon_f$) 1.2%, 0.6% and 0.35% and Vickers hardness (HV) 75 HV0.2, 95 HV0.2 and 115 HV0.2. The reference properties for Zn were UTS = 105 MPa, YS = 45 MPa, $\varepsilon_f$ = 13.5% and 35 HV0.2.

### 2.3. Hydrostatic extrusion

The hot extruded rods were then hydrostatically extruded (HE) at

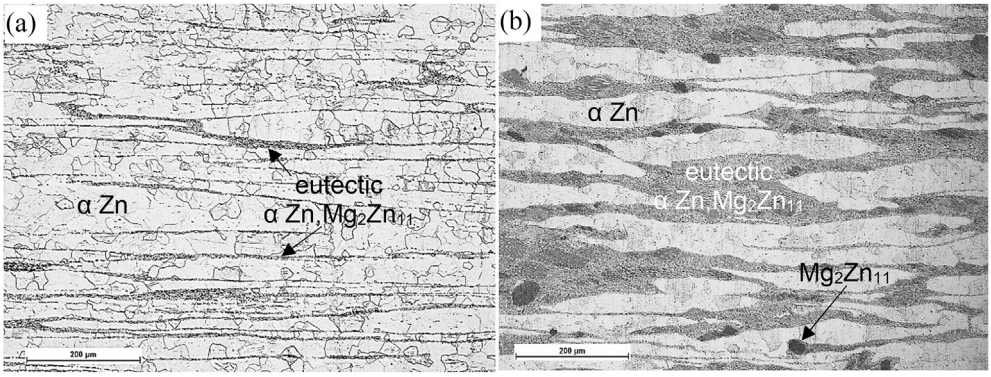


**Fig. 1.** Longitudinal microstructure of initial material after casting and hot conventional extrusion at 250 °C to rods of 30 mm in diameter (a) Zn-0.5 Mg, and (b) Zn-1.5 Mg alloy.

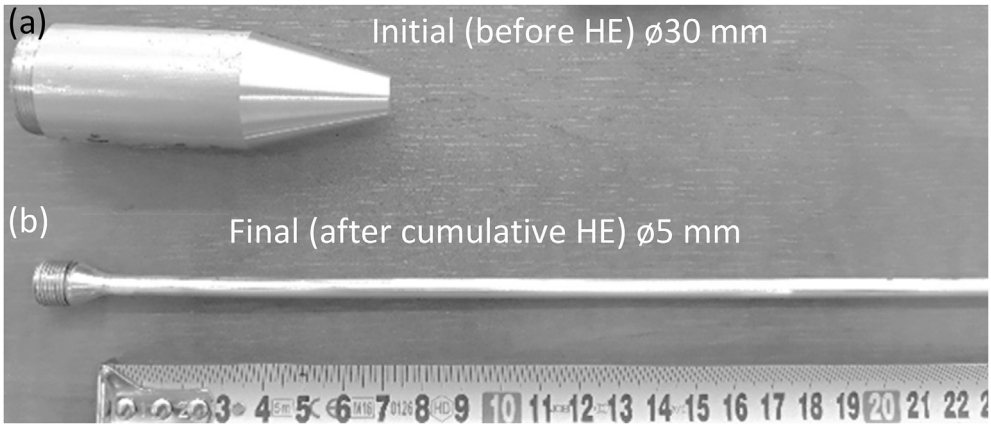


**Fig. 2.** Examples of (a) billet for hydrostatic extrusion HE made of Zn–Mg binary alloy, and (b) Zn–Mg rod after cumulative HE at room temperature.

ambient temperature with large reductions. The extrusion was performed on presses designed and built in the Institute of High Pressure Physics, Polish Academy of Science Unipress, Poland with working chamber diameters of 60 mm and 22 mm, with working pressures of 1.3 GPa and 2 GPa, respectively, and with a die angle of $2\alpha = 45°$. At the exit from the die, the rods were cooled by running cold water. The HE process was carried out cumulatively in four consecutive passes on the final diameter of the test rod of 5 mm, which corresponded to the cumulative reduction of $R_{cum} = 35$, i.e. cumulative true strain $\varepsilon_{cum} = 3.55$ and percentage strain r = 97%, Fig. 2. Linear HE extrusion speeds $v_{HE}$ were between 5.4 and 15 cm $s^{-1}$ for Zn–Mg binary alloys and 1.5–3.5 cm $s^{-1}$ for Zn, and increased with a decrease in the diameter of the extruded rod, which is equivalent to an increase in cumulative plastic deformation. Linear speeds correspond to plastic deformation strain rates in the range $\dot{\varepsilon}_{HE} = 6.8–50\ s^{-1}$ and 2.1–12 $s^{-1}$ for Zn–Mg and Zn alloys, respectively.

The structure of rods after four HE passes is presented in Fig. 3a and b. In order to modify the deformation, the number of cumulative HE passes was also shortened to two, reaching the same $\varepsilon_{cum} = 3.55$, Fig. 3c and d. The microstructure shows a high degree of texturisation with visible, strongly elongated $\alpha$Zn grains and the $\alpha$Zn + $Mg_2Zn_{11}$ eutectic stretched longitudinally between them. For the Zn-0.5 Mg alloy, the distribution of eutectic in the $\alpha$Zn matrix is less uniform, Fig. 3a, compared to Zn–1Mg and Zn-1.5 Mg alloys, Fig. 3b, which results from the amount of Mg alloy addition and forced uniform elongation of soft phase of $\alpha$Zn with hardness ~32 HV0.2 by surrounding hard eutectic with ultra-hard phase of intermetallic compound $Mg_2Zn_{11}$ ~ 383.4 HV (3.76 GPa) with the most reduced module 108.94 GPa [22]. Comparing 4 to 2-pass HE, the thicker bands of the $\alpha$Zn + $Mg_2Zn_{11}$ eutectic in the second case are noticeable, which can be attributed to the almost 2 times higher deformation in the first HE pass, which does not allow for refinement of the eutectic during the second pass due to a significant increase in defect density and strain hardening of the material. In addition, higher extrusion pressures during 2-pass HE reduce defects mobility and diffusion effects in the deformed material.

The dependence of the extrusion pressure $p_{HE}$ as a function of plastic deformation $\varepsilon$ for the HE process at ambient temperature for Zn and three Zn–Mg binary alloys extruded with 1 and 4 passes in a cumulative manner is presented in Fig. 4. The HE characteristics for one pass reflect the well-known linear relationship of $p_{HE}$ increase with $\varepsilon$ resulting from the increase in strain hardening of the material [23]. The extrusion pressures increase rapidly with $\varepsilon$, more mildly for Zn, and strongly limit the possibility of generating a large $\varepsilon$ in the material due to the available working pressure range of the press and the melting of the samples as a result of the strong adiabatic heating (AH) effect of the deformed material (see Chapter 2.4.).

It is critical for the HE process that the extrusion takes place under stable conditions at constant pressure, which determines a constant extrusion speed. The process stability is determined by a number of independent process parameters, such as selected R, $2\alpha$, $\dot{\varepsilon}_{HE}$, volume of the pressure medium and initial plasticity of the material determined by its structure. Parameters selected for Zn and Zn–Mg binary alloys to obtain linear pressure characteristics allowed the determination of true $\varepsilon$ achievable for each alloy in a single HE pass:

$$p_{HE}^{Zn-1.5Mg} = 277.19867 + 224.47209\,\varepsilon \text{ for alloy } Zn - 1.5Mg \quad (1)$$

$$p_{HE}^{Zn-1Mg} = 202.58459 + 227.60956\,\varepsilon \text{ for alloy } Zn - 1Mg \quad (2)$$

$$p_{HE}^{Zn-0.5Mg} = 125.38788 + 243.30421\,\varepsilon \text{ for alloy } Zn - 0.5\,Mg \quad (3)$$

$$p_{HE}^{Zn} = 72.22638 + 149.5724\,\varepsilon \text{ for Zn} \quad (4)$$

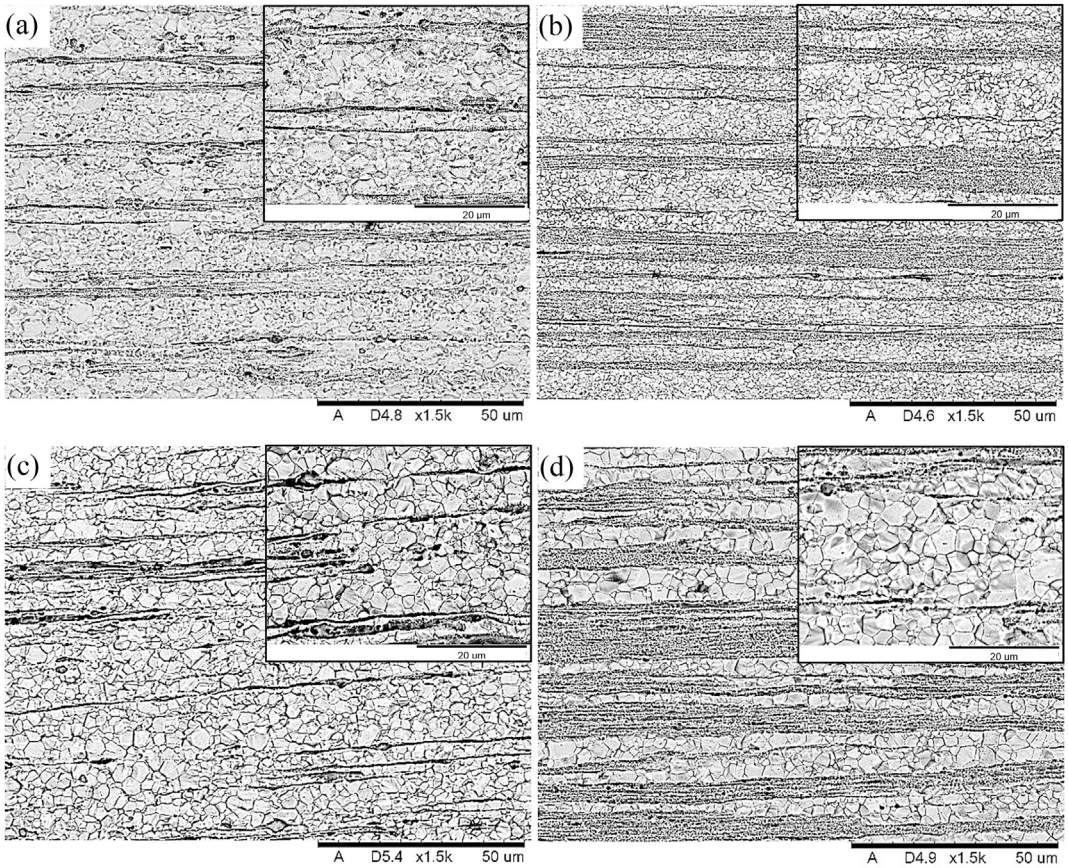


**Fig. 3.** Comparison of longitudinal microstructure of (a,c) Zn-0.5 Mg and (b,d) Zn-1.5 Mg rods after room temperature cumulative hydrostatic extrusion with cumulative true strain $\varepsilon_{cum}$ = 3.55 (reduction R = 35, percentage deformation r = 97%) in (a,b) 4-passes, and (c,d) 2-passes; Note: insets show higher magnification.

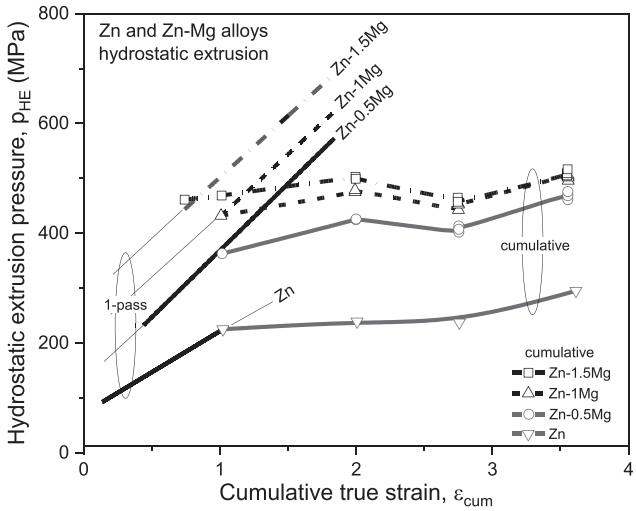


**Fig. 4.** Dependence of the extrusion pressure on true strain at room temperature hydrostatic extrusion of Zn and Zn–Mg binary alloys.

### 2.4. Adiabatic heating effect

The limitation of the applicable degree of deformation results directly from the effect of strong adiabatic heating (AH) caused by the mechanical work of plastic deformation during HE, activating the recrystallisation and increase of grain size that reduce the strain hardening of the material. This effect can even cause melting of the extruded sample. The work of plastic deformation per unit volume during HE is equal to $p_{HE}$, hence the increase in material temperature can be estimated on the basis of a commonly accepted relationship [24,25]:

$$\Delta T = \beta \frac{W}{c\,\rho} = \beta \frac{p_{HE}}{c\,\rho} \quad (5)$$

where W is the plastic deformation work per unit volume carried out during HE, $p_{HE}$ is the extrusion pressure, $c$ and ρ – specific heat and density, and $\beta$ is the proportion of work converted to heat. For the HE process carried out with a relatively high strain rate and a well insulating grease film around the working zone, $\beta$ = 0.95 can be adopted. Hence, AH temperature estimated according to equation (5) for alloy Zn-1.5 Mg and alloy properties ρ = 6.81 g cm$^{-3}$, $c$ = 0.346 J g$^{-1}$ K$^{-1}$, melting point $T_m$ = 385 °C and range of $p_{HE}$ = 455 MPa–720 MPa, Fig. 4, are between 190 and 290 °C, i.e. $T/T_m$ = 0.7–0.85, where $T/T_m$ is the homologous temperature, $T$ is the sample temperature and $T_m$ is the melting temperature, both in $K$. Similarly, for the Zn–1Mg alloy and the relevant data, the AH temperature range is 175–275 °C ($T/T_m$ = 0.66–0.81) and for the Zn-0.5 Mg alloy the AH temperature range is between 125 and 225 °C ($T/T_m$ = 0.58–0.71). For Zn the AH effect is lower – 77–100 °C ($T/Tm$ = 0.51–0.54). The data clearly show that in order to obtain high mechanical properties after HE in Zn–Mg binary alloys, the AH effect as an adverse phenomenon should be limited as much as possible. For this reason, 1-pass HE was carried out with deformations not exceeding ε = 1.85, i.e. with reductions of R < 6.3, resulting in $p_{HE}$ not exceeding 230 MPa for Zn and 570 MPa, 620 MPa and 720 MPa for Zn–Mg binary alloys, respectively with increasing Mg addition. An additional limitation of the adiabatic heating effect was favoured by the use of the lowest possible $v_{HE}$ below 2.3 cm s$^{-1}$ for Zn and below 7.3 cm s$^{-1}$ for Zn–Mg binary alloys, which corresponded to $\dot{\varepsilon}_{HE}$ below 2.1 s$^{-1}$ for Zn and 6.8 s$^{-1}$ for Zn–Mg binary alloys.

In order to reduce the thermal effect and increase the degree of deformation, cumulative HE was used, using several extrusion passes,

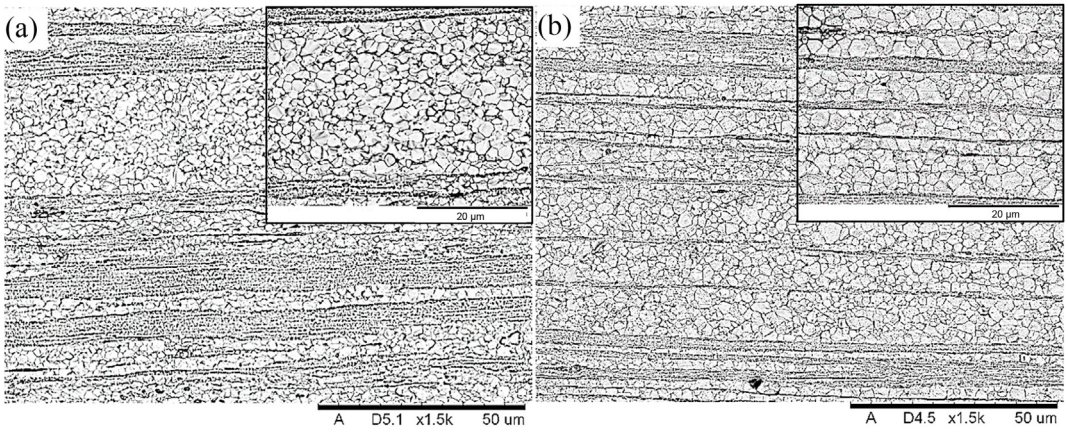


**Fig. 5.** Longitudinal microstructure of Zn–1Mg rods after cumulative hydrostatic extrusion in 2-passes with total true strain $\varepsilon_{cum}$ = 3.55 (a) at room temperature, and (b) after cryo hydrostatic extrusion. Note: Insets show higher magnification.

each with a much lower strain per pass, Fig. 4. Therefore, regardless of the type of material, it became possible to generate 2 times higher, compared to 1-pass extrusion, cumulative true strain $\varepsilon_{cum}$ ~3.6, with $p_{HE}$ reduced by ~30% (for example, for Zn-1.5 Mg from 720 MPa to 520 MPa). This significantly reduced the effect of adiabatic heating, for example for Zn-1.5 Mg from 290 °C to 205 °C, i.e. a decrease in $T/T_m$ from 0.85 to 0.73, which inhibited the recrystallisation process, increased the refinement of the microstructure, and consequently led to higher mechanical properties, UTS = 465 MPa vs. 410 MPa and YS = 355 MPa vs. 325 MPa.

### 2.5. Cryo-hydrostatic extrusion

In order to limit the thermal effect, a series of 2 and 4-pass HE was carried out, with comparable parameters as for HE at ambient temperature, of billet cooled before HE with liquid nitrogen $LN_2$. However, the first HE pass was also carried out at ambient temperature. The cryo-HE cycle included immersion of the billet in $LN_2$ for at least 45 min, loading into the working chamber, flooding the chamber with a pressure transmitting medium cooled to −30 °C and start of HE, the last three operations lasting ~10 s. Fig. 5 shows a comparison of the microstructure of Zn–1Mg alloy after 2-pass HE with $\varepsilon_{cum}$ = 3.55 (a) in ambient atmosphere, and (b) after cryo-deformation. In the 'cryo' sample (b) a more homogeneous and higher texturisation is seen, resulting in the eutectic $\alpha$Zn + $Mg_2Zn_{11}$ being stretched into thinner bands along the $\alpha$Zn grains and finer grains – $d_{eq}$ = 2.1 μm vs. 3.2 μm (a). Both of these factors led to a significant hardening of the material after cryo-deformation UTS = 423 MPa vs. 367 MPa and YS = 369 MPa vs. 327 MPa MPa with comparable plasticity $\varepsilon_f$~ 35% and hardness ~108 HV0.2.

### 2.6. Combined hydrostatic extrusion with ECAP

In order to check if microstructure refinement before HE by equal channel angular pressing ECAP (herein after ECAP + HE) can additionally increase the strength and plasticity of Zn–Mg binary alloys for Zn-0.5 Mg, a 2-pass ECAP process was carried out with a subsequent 2-pass HE process. Before the ECAP and HE processes, the output samples were annealed to homogenize and soften the structure. The annealing included three temperatures of 150 °C, 250 °C and 350 °C, and three times – 0.5, 1 and 4 h for each temperature. The samples, after annealing in the air, were cooled with water or cooled freely in open air. The microstructure after annealing is presented in Fig. 6. For Zn-0.5 Mg, regardless of the time, at 150 °C the texture of the initial material was maintained after hot extrusion with slight increase of $\alpha$Zn grains, leading to the lowest hardness of 67 HV0.2, Figs. 6a and 1a. At a temperature of 350 °C, total recrystallisation and increase of $\alpha$Zn grains to the size of hundreds of micrometers with the $\alpha$Zn + $Mg_2Zn_{11}$ eutectic distributed on their circumference and increase in hardness to 103 HV0.2, i.e. by more than 50% in comparison with the temperature of 150 °C, was observed, Fig. 6b. Therefore, before the HE and ECAP + HE processes, the samples were annealed at 150 °C for 4 h by cooling in water, leading to a maximum softening of 13% compared to the initial hardness. The billets for ECAP were square 9.5 × 9.5 mm and for HE – round 10 mm, in order to obtain the same cumulative reduction of $R_{cum}$ = 3.6. All processes were conducted at ambient temperature. The ECAP process was carried out with a 90° channel angle using the 'C' method at a linear rate of 0.07 mm $s^{-1}$, which corresponded to plastic deformation rate $\dot{\varepsilon}_{ECAP} = 4.46 \times 10^{-2}\ s^{-1}$ and true strain after 2 ECAP passes $\varepsilon_{ECAP}$ = 1.93. After adding the 2-pass HE, the cumulative strain amounted to $\varepsilon_{cum}^{ECAP+HE}$ = 3.22., the cumulative strain for 2-pass HE was $\varepsilon_{cum}^{HE}$ = 1.28, and the AH temperature calculated according to equation (5) did not exceed 140 °C corresponding to $T/T_m$ < 0.59.

Carrying out the ECAP process before the HE process resulted, compared to HE alone, in a significant improvement of the texture and grain size distribution by 2.5 times, increasing the accumulated $\varepsilon_{cum}$ and changing the flow paths of the material. The eutectic fibres with an ultra-hard $Mg_2Zn_{11}$ intermetallic phase were thinner, evenly distributed and stretched to form a stable skeleton, effectively fragmenting and strengthening the matrix made up of soft phase $\alpha$Zn, Fig. 7. This resulted in a more than 25% increase in UTS, 28.5% increase in YS, 18% increase in HV, and most importantly, an over 15% increase in $\varepsilon_f$. However, in comparison with 4-passes HE at room temperature, the results after ECAP + HE were significantly lower, due to higher $\varepsilon_{cum}$ and less developed texture, see Fig. 3b.

### 2.7. Uni-axial compression

The properties obtained in the static compression test for one and a half time samples with a diameter of 5 mm were, respectively, Zn-0.5 Mg, Zn–1Mg and Zn-1.5 Mg: compressive yield strength $\sigma_{d0.2}$ = 185 MPa, 315 MPa, and 370 MPa, and at compressive strength at 80% strain $\sigma_{dM}$ = 1280 MPa, 1410 MPa i 1590 MPa. Analogous properties for Zn were $\sigma_{d0.2}$ = 70 MPa and $\sigma_{dM}$ = 755 MPa. The strain at compression strength for all samples was equal and amounted to $\varepsilon_{dM}$ = 72%. As mentioned above, the compression process could be continued without any signs of sample cracking.

## 3. Results and discussion

### 3.1. Microstructure after HE

Irrespective of HE conditions, the microstructure of Zn–Mg binary alloys in comparison with the initial materials shows a strong degree of

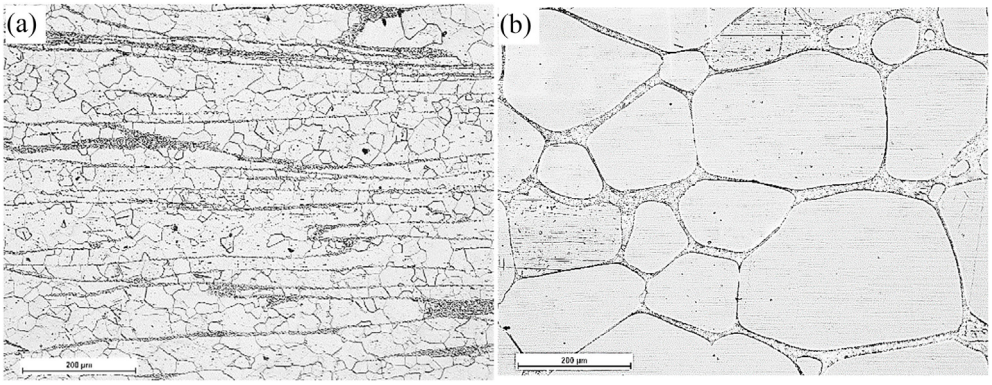


**Fig. 6.** Longitudinal microstructure of Zn-0.5 Mg after annealing of the initial, as received state by 4 h in air and cooled in cold water at (a) 150 °C, 67 HV0.2 and (b) 350 °C, 101 HV0.2.

elongation of $\alpha$Zn grains and surrounding eutectic areas $\alpha$Zn + $Mg_2Zn_{11}$ in the extrusion direction, Figs. 3, 6 and 7, and a large refinement of the microstructure, Fig. 8. After $\varepsilon_{cum}$ = 3.55, the average $d_{eq}$ grain size in the longitudinal section in the HE direction is respectively for Zn, Zn-0.5 Mg, Zn–1Mg and Zn-1.5 Mg: 16 μm, 2.3 μm, 1.5 μm and 1.6 μm. Dark areas on IPF maps containing the $Mg_2Zn_{11}$ intermetallic phase with $\alpha$Zn nano-grains were not taken into account for $d_{eq}$ calculations. Increasing the content of Mg leads to a gradual reduction of $d_{eq}$, especially in the lower range of the alloying agent. The increase in refinement results from the increase in the volume of the $\alpha$Zn + $Mg_2Zn_{11}$ eutectic, Fig. 9, containing the $Mg_2Zn_{11}$ hard intermetallic phase, isolating large areas of the pure, more ductile $\alpha$Zn phase, which inhibits their increase. The dependence of $d_{eq}$ on $\varepsilon_{cum}$ for Zn–Mg binary alloys is presented in Fig. 10. The grain size on the longitudinal section is slightly higher compared to the cross-section and decreases strongly for the first two HE passes, slowly stabilising in the further two, above $\varepsilon_{cum}$ ~2. Grain refinement in the first two passes of HE occurs more strongly and to a lower level for alloys with a higher Mg content compared to Zn-0.5 Mg, which is due to the higher number of defects generated and lower mobility of grain boundaries.

### 3.2. Mechanical properties after HE at room temperature

Refinement of the microstructure during plastic deformation is crucial for the mechanical properties of the obtained material. The dependence of mechanical properties of Zn–Mg binary alloys on $\varepsilon_{cum}$ for HE at ambient temperature is presented in Fig. 11. The sensitivity to the degree of plastic deformation is highest for Zn-0.5 Mg, which is, among others, the result of the lowest strength properties of UTS and YS of the alloy in the initial state before HE. Hardening, in comparison with the initial material after maximum $\varepsilon_{cum}$ = 3.55, increased for Zn-0.5 Mg, Zn–1Mg and Zn-1.5 Mg alloys, respectively, for UTS by

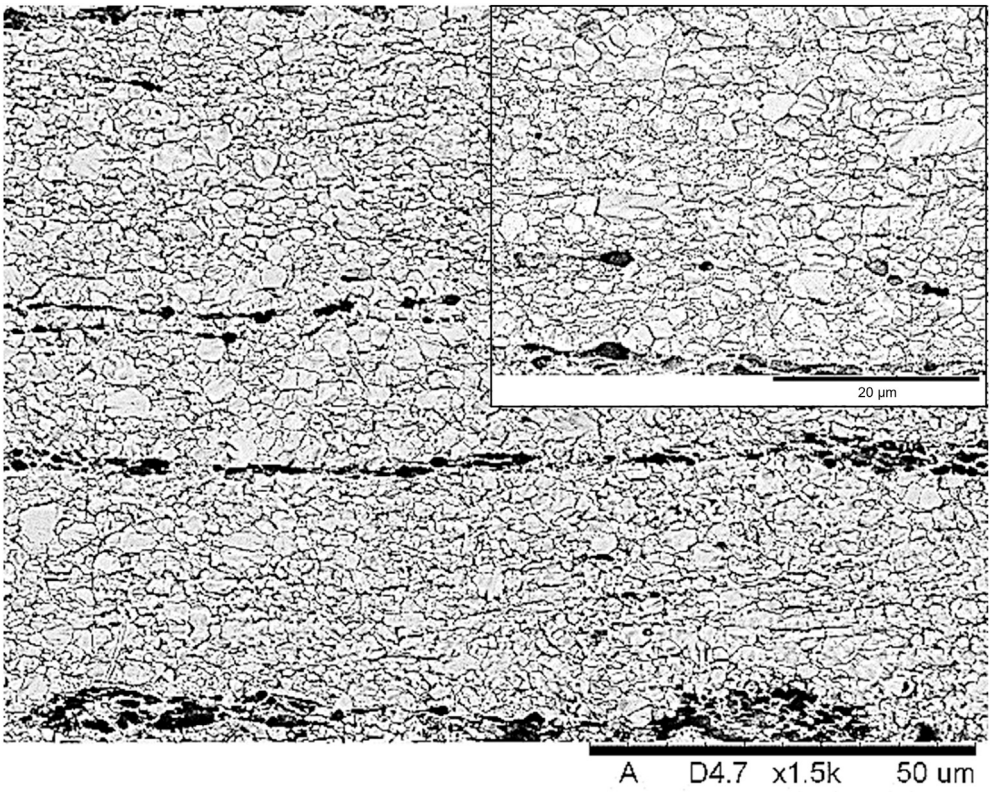


**Fig. 7.** Longitudinal microstructure of Zn-0.5 Mg rod after 2-passes of ECAP followed by 2-passes of room temperature hydrostatic extrusion with cumulative true strain $\varepsilon_{cum}$ = 3.22; Note: inset shows higher magnification.

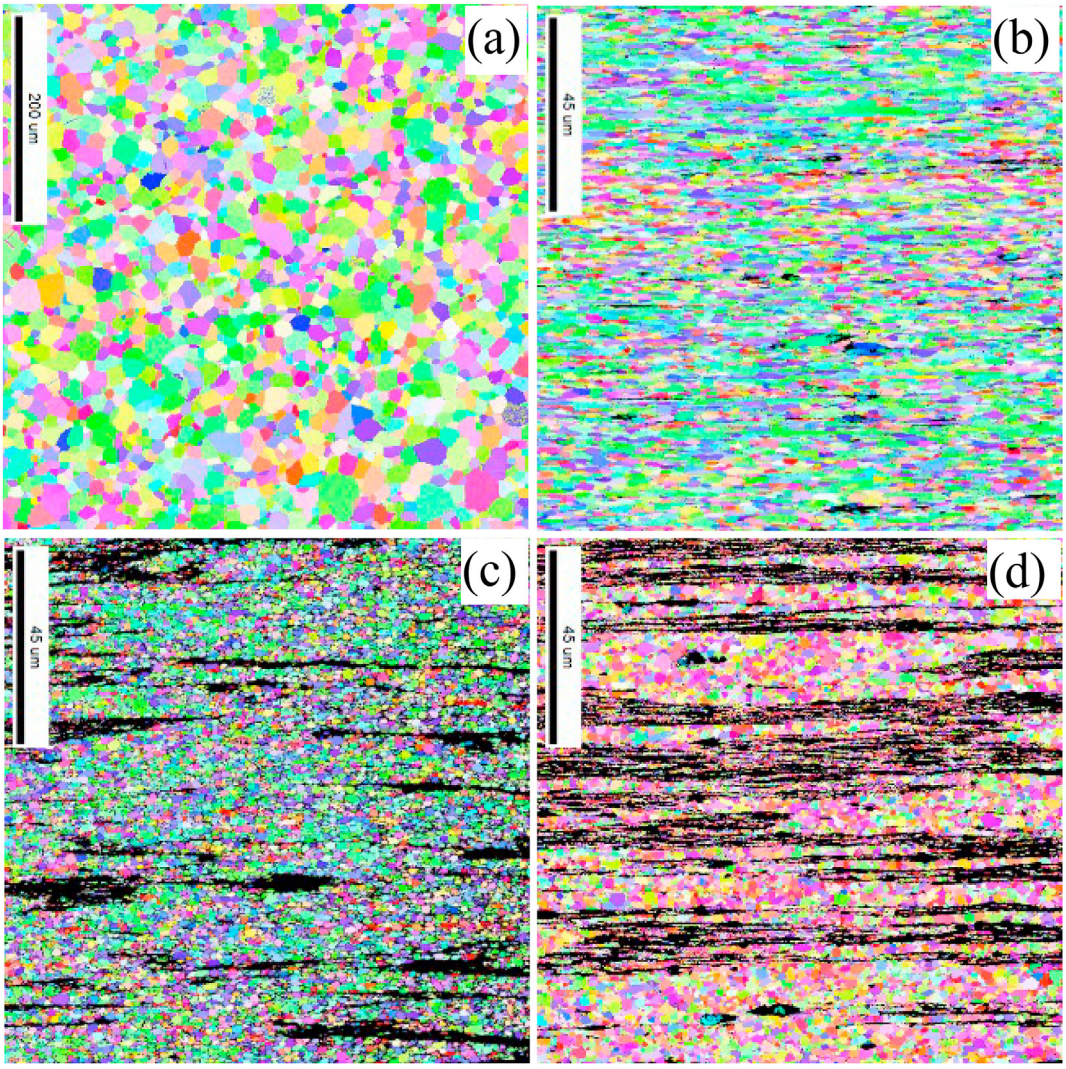


**Fig. 8.** IPF maps of the EBSD data analysis for the longitudinal sections after 4-passes room temperature hydrostatic extrusion with cumulative true strain $\varepsilon_{cum}$ = 3.55 of (a) Zn, (b) Zn-0.5 Mg, (c) Zn–1Mg and (d) Zn-1.5 Mg.

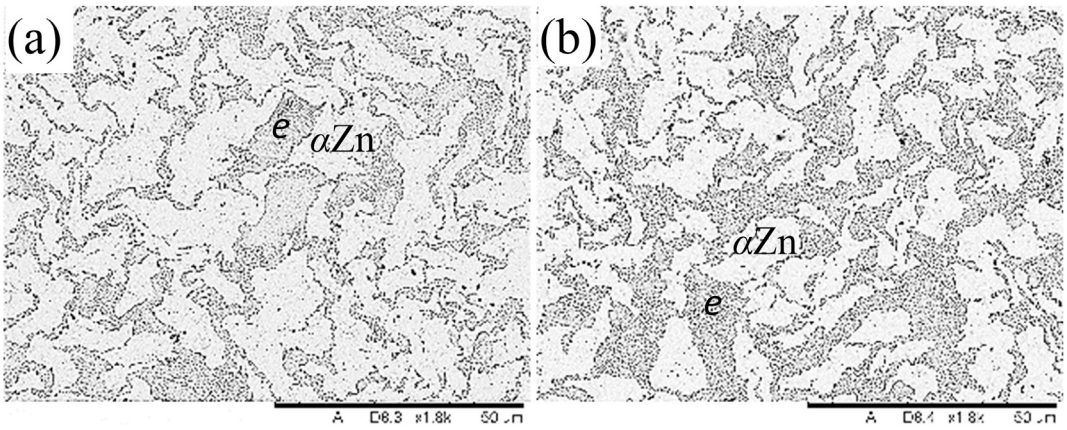


**Fig. 9.** SEM microstructures of transverse sections after 4-passes room temperature hydrostatic extrusion with cumulative true strain $\varepsilon_{cum}$ = 3.55 of (a) Zn–1Mg and (b) Zn-1.5 Mg; Note: *e* denotes eutectic *α*Zn + $Mg_2Zn_{11}$ areas.

168%–515 MPa, by 55%–480 MPa and by 36%–465 MPa and for YS by 150%–375 MPa, by 62%–365 MPa and by 29%–355 MPa. Plasticity is preserved similarly to strength, showing increases in elongation to fracture $\varepsilon_f$, starting from the lowest alloy, respectively, up to 10.5%, 25% and over 38%, i.e. ~ 9-fold, over 40-fold and over 100-fold, Fig. 11.

Vickers hardness also increases but on a much smaller scale compared to strength changes, Fig. 12. The hardnesses after HE increase with the increase of the alloying addition and reach at maximum $\varepsilon_{cum}$ values of 105, 115 and 120 HV0.2, respectively. What is striking is the

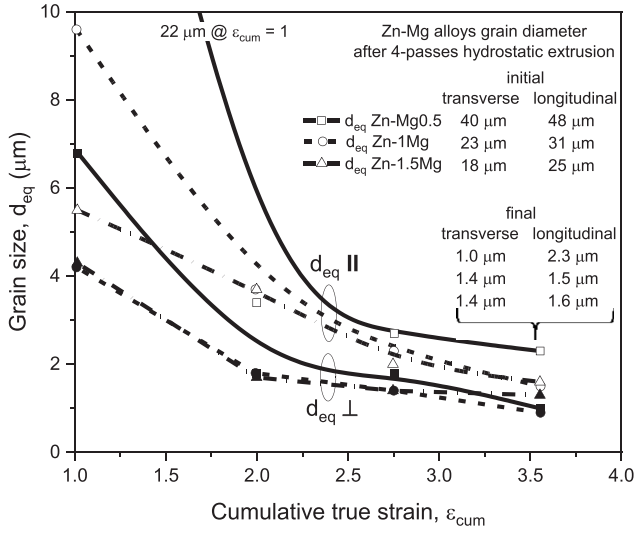


**Fig. 10.** Grain size variations with true strain at room temperature cumulative hydrostatic extrusion of Zn–Mg binary alloys.

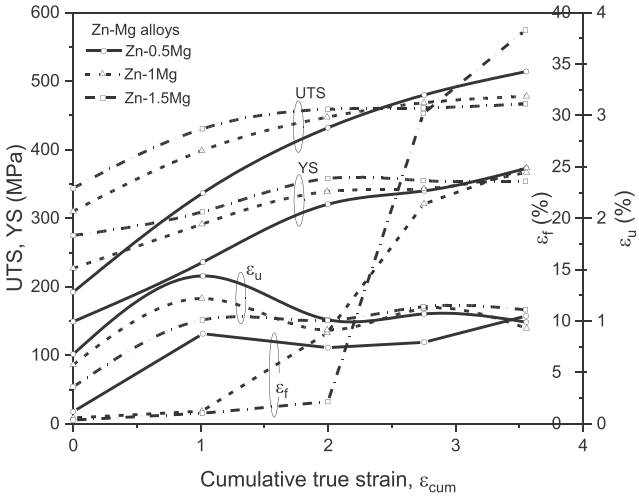


**Fig. 11.** Tensile properties of Zn–Mg binary alloys after 4-passes room temperature cumulative hydrostatic extrusion.

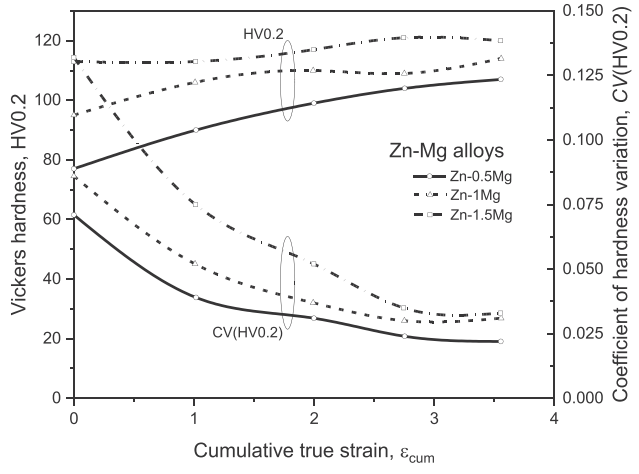


**Fig. 12.** Vickers hardness of Zn–Mg binary alloys after 4-passes room temperature cumulative hydrostatic extrusion.

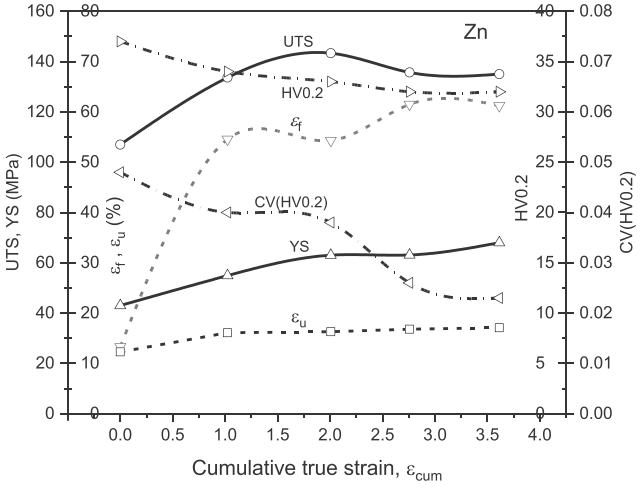


**Fig. 13.** Tensile properties and Vickers hardness of Zn after 4-passes room temperature cumulative hydrostatic extrusion.

clear homogenisation of the microstructure during the HE processes, as presented by the decrease in the coefficient of variation of hardness CV (HV0.2), equal to the ratio of standard deviation to mean value, already after the first HE pass and its stabilisation at the last two passes of deformation. These changes are more pronounced for the highest alloy Zn-1.5 Mg, which results from the greatest structural heterogeneity in this alloy.

Zn hardening is much milder, and HV even drops with an increase in $\varepsilon_{cum}$, Fig. 13. This is confirmed by a strong AH effect, in the range 0.51–0.55 $T/T_m$ (77–107 °C), increasing with an increase in $\varepsilon_{cum}$ to induce the recrystallisation processes in the material. This results in a rapid saturation of the cumulation of deformation-generated defects and the beginning of their annihilation, leading to a decrease in strength after the second pass of HE, as presented by UTS in Fig. 13. Compared to the initial material, after maximum $\varepsilon_{cum}$, UTS for Zn increases by 26%, YS by almost 60%, elongation to fracture $\varepsilon_f$ by 360%, and HV hardness decreases by 14%. The last two values clearly indicate the susceptibility of Zn to thermal softening processes caused by AH.

### 3.3. Mechanical properties' dependence on the number of cumulative deformation processes

From the point of view of future applications of Zn–Mg binary alloys, the reduction in the number of deformation passes reduces the costs associated with the manufacture of prefabricated elements for implants. Hence, 4-pass HE was replaced by 2-pass HE. Fig. 14 shows a comparison of HV of Zn–Mg binary alloys with 4-pass (*columns*) and 2-pass (*black dots*) HE at ambient temperature with this $\varepsilon_{cum}$ and for the same final diameter of 5 mm. Regardless of the type of alloy, Zn–Mg 2-pass HE always leads to lower final HV compared to 4-pass, and the difference decreases with the increase of alloying additive Mg. Lower HV between 3 and 22% is due to larger ε per one pass with fewer operations, and therefore higher AH effect during HE ~220 °C vs. 165 °C for Zn-0.5 Mg, ~275 °C vs. 205 °C for Zn–1Mg and ~290 °C vs. 205 °C for Zn-1.5 Mg. What was to be expected is that HV decreases correspond to adequate UTS and YS decreases, the highest for the purest alloy Zn-0.5 Mg for UTS by ~36% and YS by ~17%, and the lowest for the highest alloy Zn-1.5 Mg for UTS by ~12% and YS by ~9%. Interestingly, the limitation to 2 passes of HE is accompanied by a significant increase in $\varepsilon_f$ plasticity, drastic for Zn-0.5 Mg by almost 150% and significant for Zn–1Mg by almost 50%. On the other hand, Zn-1.5 Mg alloy with the highest density of defects and obstacles to dislocation movement, i.e. factors inhibiting the annihilation of defects and grain increase, shows an almost 30% decrease in plasticity. Fig. 14 demonstrates that with the appropriate size selection of ε, the HE process

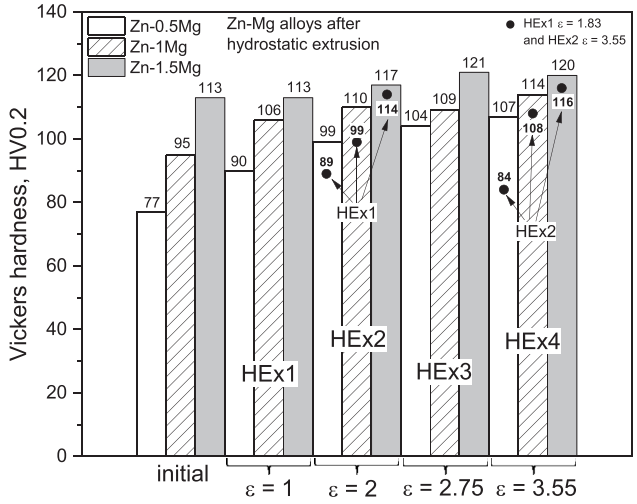


**Fig. 14.** Comparison of HV dependences on true strain between 4-passes and 2-passes room temperature cumulative hydrostatic extrusion of Zn–Mg binary alloys.

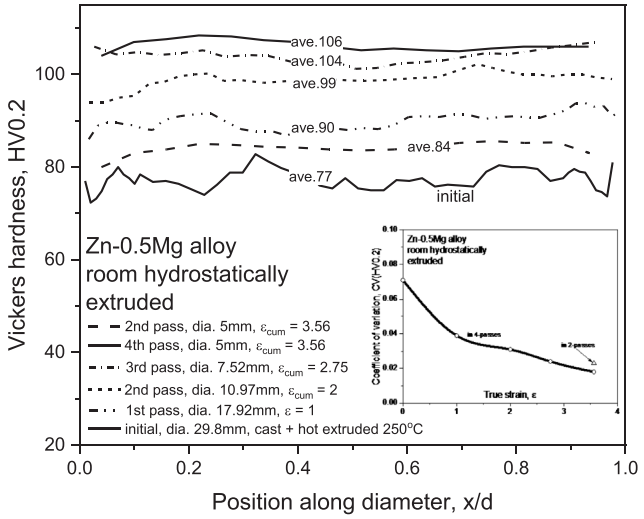


**Fig. 15.** Distribution of Vickers hardness along the rod diameter after room temperature cumulative hydrostatic extrusion of Zn-0.5 Mg alloy; Note: inset presents the dependence of HV coefficient of variation on the true strain ε.

enables a wide HV range for Zn–Mg binary alloys between 85 and 120 HV0.2. However, as the results obtained show, in order to obtain Zn–Mg binary alloys of high hardness and strength, reducing the number of cumulative HE passes becomes unfavourable.

### 3.4. Hardness distribution across the extruded wire (structural homogeneity)

One of the most important features of the HE process is the ability of extrusion through low angle conical dies. This is made possible by supporting the external cylindrical surface of the die with a high hydrostatic pressure compensating for the pressure acting on the internal conical surface of the die in contact with the extruded material. The low angles 2α of the dies reduce the deformation of the strain grid by lowering the so-called "redundant work" performed perpendicularly to the direction of extrusion, as a result of which the billet cylinder transforms into a rod cylinder, similar to what happens during uni-axial tensile test. This promotes the transverse homogeneity of the extruded material and, as a result, the homogenisation of mechanical properties on the cross-section of the extruded product. This effect is also strongly favoured by cumulative HE in several passes with smaller unit ε per pass. This is clearly illustrated by the HV0.2 transverse hardness distribution for the Zn-0.5 Mg alloy in Fig. 15. The heterogeneous distribution of HV after casting and conventional hot extrusion 77 HV0.2 (*solid*) clearly increases and equalises its distribution to 106 HV0.2 on the rod cross-section after 4 HE passes. A clear decrease in the CV (HV0.2), presented in the insert in Fig. 15, indicates the homogeneity of the properties across the extruded rod. The remaining Zn–Mg binary alloys behave similarly, except that the increase range of HV between the initial material and after pass 4 of HE is narrowed down with the increase of Mg addition by 29 units for Zn-0.5 Mg (77 → 106 HV0.2), 12 units for Zn–1Mg (95 → 107 HV0.2) and 7 units for Zn-1.5 Mg (113 → 120 HV0.2), respectively. This may be due to a decrease in mobility of dislocation in material with a higher content of hard eutectic phase. Cryo-HE causes a 50% increase in HV 77 → 116 HV0.2 compared to room temperature. This is due to the greater refinement of the microstructure and the higher density of structural defects generated at much lower temperatures. Although in both cases the final homogeneity of HV distribution approaches similar values, the homogenisation of the structure at room temperature is milder compared to the intermediate passes of cryo-deformation.

The maintenance of highly fragmented structural and mechanical uniformity in the cross-section of the extruded rod may be of great importance if, in order to maintain appropriate hardness, hot extrusion of tubes [7] is replaced with tubes obtained from cold HE of rod with subsequent drilling of the hole and laser cutting or pickling of the mesh. The benefits may be significant if one compares the properties for hot processed alloy Zn-0.5 Mg [7] with cold HE method, see Chapter 3.13., Table 2, UTS = 300 vs. 515 MPa, YS = 160 vs. 375 MPa and 65 HV vs. 105 HV, or for the Zn–1Mg alloy: UTS = 340 vs. 480 MPa, YS = 180 vs. 365 MPa, $\varepsilon_f$ = 6 vs. 25% and 75 HV vs. 110 HV. This is due to the fact that hot treatment allows the obtaining of grain refinement above 4 μm for the extrusion of Zn-0.5 Mg [7] or 6–7 μm for the extrusion and drawing of Zn-(0.005–0.08)Mg [13]. Additionally, hot working leads optionally to very high heterogeneity of the structure with the $Mg_2Zn_{11}$ intermetallic layer concentrated near the wire axis [13]. The HE process allows the maintenance of a high grain refinement of ~2 μm and the maintenance of high mechanical properties and plasticity on the perimeter of the rod from which stents can be formed.

Low-angle dies cause that during the deformation in the HE process at the exit of the die, the material of the core of the rod does not significantly advance the area around its circumference. This promotes the reduction of shear stress in the material and the obtaining of equiaxial grains in the cross-section, which for alloy Zn–1Mg and die angle 2α = 45° is illustrated by Fig. 16. The material on the perimeter of the rod shows a significantly higher degree of refinement compared to the core, due to a stronger AH effect and slower cooling for the last one. The other Zn–Mg binary alloys behave similarly.

### 3.5. Combination of deformation processes

A combination of different forming methods is used to multiply the ε intensity of the material by changing the deformation path and increasing the degree of refinement of its structure. The severe plastic deformation (SPD) method leads to the generation of ultra-fine (UFG) and nanocrystalline (NC) structures in such materials as Cu, CuCrZr and Ni [26,27]. For the Zn-0.5 Mg alloy, the addition of ECAP as a preliminary deformation before HE, due to the increase in $\varepsilon_{cum}$, led to an increase in all mechanical properties, see Chapter 2.6, including an increase of more than 20% in yield strength at uni-axial compression $\sigma_{0.2}$. Compared to the initial material, YS grow less by ~100% in tension than $\sigma_{0.2}$ in compression by ~140%, while increases in ECAP + HE compared to HE for the same values are 30% for YS and 20% for $\sigma_{0.2}$. This is due to the addition of an ECAP process with a different deformation path and the synergistic effect of greater refinement and homogenisation of the microstructure, as indicated by a significant

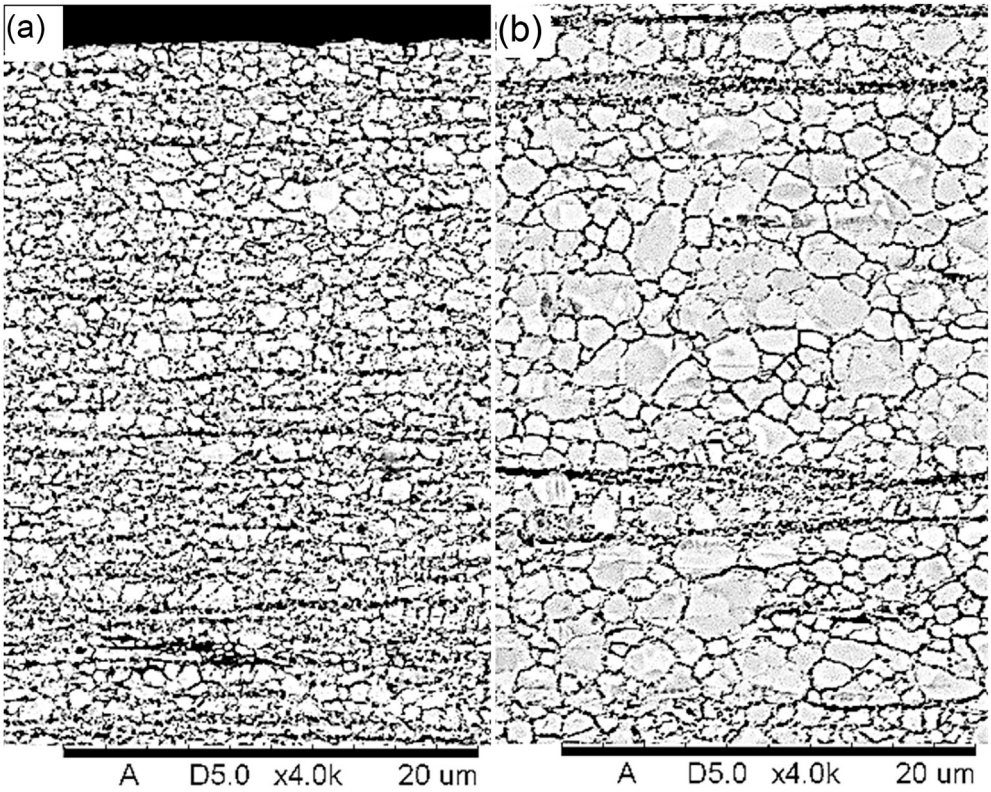


**Fig. 16.** SEM longitudinal microstructure of Zn–1Mg alloy after room temperature hydrostatic extrusion to 5 mm rod with cumulative true strain $\varepsilon_{cum}$ = 3.55 (a) at the circumference, and (b) within the core, average grain size 0.9 ± 0.5 μm; Note: similar distribution was observed in other Zn–Mg binary alloys.

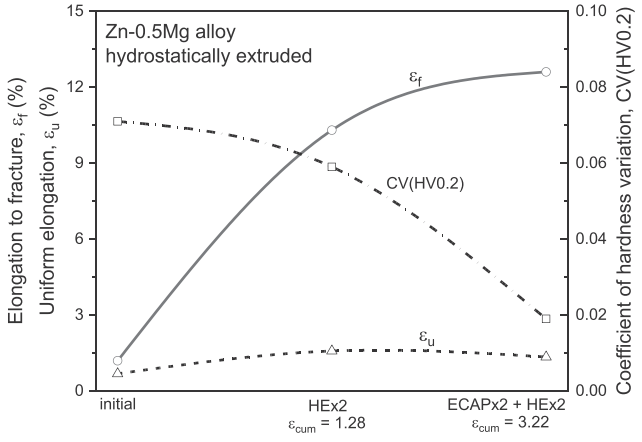


**Fig. 17.** Comparison of elongation to fracture $\varepsilon_f$, uniform elongation $\varepsilon_u$ and coefficient of hardness variation CV(HV0.2) in Zn-0.5 Mg alloy after 2-passes room temperature cumulative hydrostatic extrusion and 2-passes of ECAP by C procedure followed by 2-passes room temperature cumulative hydrostatic extrusion. Note: properties of initial material before deformation are given for reference.

decrease in the CV(HV0.2), Fig. 17. From the point of view of subsequent applications, it is important to increase the $\varepsilon_f$ plasticity of the Zn–Mg binary alloy, from which, e.g. a stent is to be made, due to its continuous operation. The presented results show a positive effect for Zn–Mg binary alloys of combining mixed strain techniques leading to an increase in mechanical properties determined by hardness, static tension and uni-axial compression measurement methods.

### 3.6. Cryo-deformation

It is commonly known that cryo-deformation applied to materials deformed by different SPD processes allows the obtaining of, both in pure materials and their alloys, highly refined UFG or NC structures [28–31]. From the point of view of cryo-deformation, the HE process is particularly privileged, which, thanks to its 3-axial compressive stress, allows the material to remain cohesive even with very large unit ε, which results in increased mechanical properties. Cryo-HE used for Cu refined the structure by 30% more strongly compared to ε at room temperature, which resulted in a dramatic increase in YS by 380%, UTS by 90% and HV by 185% [32]. This effect is generated by a decrease in the dislocation mobility combined with an increase in their density.

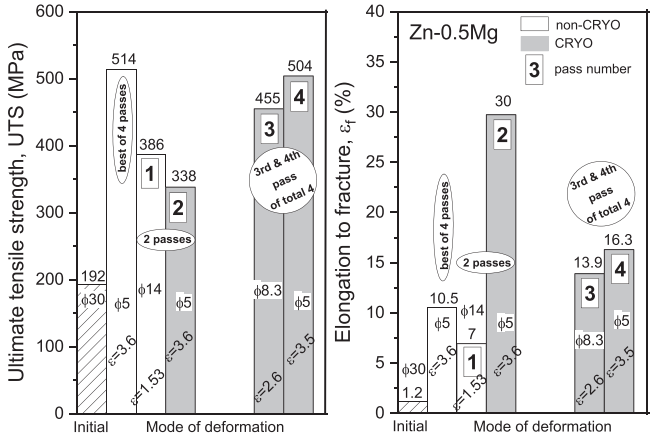


**Fig. 18.** Zn-0.5 Mg alloy (a) the ultimate tensile strength UTS and (b) the elongation to fracture $\varepsilon_f$ after 4-passes cumulative hydrostatic extrusion HE conducted at room temperature (*blank*) and after single and cumulative HE at the liquid nitrogen temperature (*grey*), both with water cooling at the die exit. Note: properties of initial materials before deformation (*sparse*) are given for reference.

Fig. 18 shows the juxtaposition of UTS and $\varepsilon_f$ of the Zn-0.5 Mg alloy after cumulative cryo-HE (*filled columns*) with the best HE results at room temperature (*empty columns*). Although the use of cryo-HE, for the 4-pass extrusion, leads to a comparable UTS, Fig. 18a, the real benefit of using cryo-HE compared to room temperature lies in the drastic increase of $\varepsilon_f$, already after the 2nd cryo-HE, to 30%, i.e. by 185% compared to room temperature, and to 16% after the 4th cryo HE, i.e. by over 50%, Fig. 18b. For the Zn–1Mg alloy the value of $\varepsilon_f$ after the 2nd cryo-HE increased to 35%, i.e. by 40% in comparison with room temperature. Therefore, taking into account the possible applications of Zn–Mg binary alloys, it should be remembered that the highest final plasticity is obtained when their cryo-HE process is incorporated into the processing path.

The highest hardness HV0.2 among 0.5% and 1.0% alloys was 116 HV0.2 after 4 passes of cryo-HE alloy Zn-0.5 Mg. It was higher by ~10% compared to room temperature, while in the Zn–1Mg alloy, all cryo-HE combinations had lower HV than room temperature 110 HV0.2. This can be attributed to a much higher AH effect for the Zn–1Mg alloy generated during cryo-HE resulting from the reduction of the number of extrusion passes to two and the associated increase in $p_{HE}$, which brought the AH effect to a range of $T/T_m$ from *~0.7* to close to 1.0 (406 °C).

Cryo-HE has proven to be very effective in improving the final plasticity of Zn–Mg binary alloys. However, it did not significantly affect the final UTS. Cooling the billet before the cryo-HE to $LN_2$ temperature, together with cooling the product after leaving the die with water enables a partial inhibition of the dynamic and static thermal softening effects of the material. Hardening of Zn–Mg binary alloys results from the effective cumulation of defects generated during cryo-deformation and a decrease in dislocation mobility, which, when the material is subjected to the SPD process, causes a rapid transformation of the material coarse to UFG and, as a result, a significant increase in the final $\varepsilon_f$, which is the main advantage of using cryo-HE for Zn–Mg binary alloys.

### 3.7. Tension toughness

In engineering applications, metallic materials require high UTS and YS, as well as $\varepsilon_u$ and $\varepsilon_f$. In most cases, high values of both properties, strength and plasticity, are important. Ref. [33] presents a parameter called tension toughness (T) defined as $T = YS \times \varepsilon_u$. It describes the toughness of the material subjected to uni-axial tension and denotes the fracture work per unit of volume before the forming of a neck, i.e. plastic instability. More accurate values can be obtained from the area under the stress-strain curve using the trapezoidal rule, as recently described in Ref. [34,35]. The results discussed in this paper are based on the tension toughness T defined by the above formula.

As indicated, the fine-grained structure of UFG and NC is a major contributor to obtaining high mechanical properties, while micrograins are involved in the achievement of higher plasticity, which in total makes up the bimodal microstructure with increased toughness. Typical bimodal microstructure is observed in Zn–Mg binary alloys after HE: strongly elongated, micrometric grains of *α*Zn and longitudinally stretched between them – *α*Zn + $Mg_2Zn_{11}$ eutectic, surrounding UFG grains of *αZn*, Fig. 8. The voluminous increase in brittle *α*Zn + $Mg_2Zn_{11}$ eutectic causes a decrease in resistance to the development of brittle fractures [4].

A good visualisation of T is represented by SEM images made perpendicularly to the axis of the tensioned samples at the points of fracture, Fig. 19. The fractures show dimples resulting from the nucleation of the cavities, and their increase and coalescence during increase of ε at fracture. For lower $d_{eq}$, Fig. 10, the diagonals of the dimples grow, which results from the increase of YS along with the increasing refinement of the microstructure and low $\varepsilon_u$, Fig. 11, which cause the initiation of cavity nucleation and their coalescence at the lower ε and takes longer before the material cracking.

The analysis of T of Zn–Mg binary alloys covers the range of micro and submicrometer grains, in which the classical dislocation mechanism dominates during tensile deformation. Fig. 20 shows T for pure Zn and Zn–Mg binary alloys for the 16–220 μm grain range for Zn and 1–42 μm for Zn–Mg binary alloys. Toughness increases with $d_{eq}$ twice for Zn and 2.5–4 times for Zn–Mg binary alloys, and is higher at 1.16 GPa % for Zn, Fig. 20a, and lower at 0.35–0.4 GPa % for Zn–Mg, Fig. 20b, which is due to a much larger initial grain in Zn ~16 μm compared to ~1 μm in Zn–Mg binary alloys. Initial materials before HE showed low T ~0.1 GPa % for alloys and over 5 times higher for Zn.

Fractures occur with the neck and dimples characteristic of plastic or mixed brittle-plastic fractures, Fig. 19. After HE, apart from drastic hardening, there was a significant increase in plasticity, i.e. deformation to fracture $\varepsilon_f$. The inserts in Fig. 19 show the reduction of 3 mm samples thickness before fracture (*arrows*) and neck diameters just before fracture (without *arrows*). Zn after SPD shows a gigantic increase in plasticity, compared to the initial material, by more than 360%, which is presented by the high thickness reduction of the outer diameter of the sample from 3 to 1.73 mm (~67%) and, as a result, the minimum neck diameter before fracture ~ 0.25 mm, i.e. with more than 99% thickness reduction, Fig. 19a. Equiaxial grains with cleaned grain interiors, as a result of adiabatic heating during HE, are not obstacles to dislocation movement during static fracture, Fig. 21a. The situation changes dramatically in the case of Zn–Mg binary alloys, mainly as a result of significant grain refinement and hardening of the structure after SPD, Fig. 21. Fractures with clear 'dimples' are plastic in nature, with density, average size and depth increasing with the increase of the Mg content, Fig. 19b–d, and point to the mechanism of intercrystalline plastic fractures. The distribution of dimples is quite random and increases significantly with the increase of the alloying element Mg, Fig. 19b,d. This is caused by the heterogeneous distribution, depth and thickness of *α*Zn + $Mg_2Zn_{11}$ eutectic bands on sections of extruded rods, Fig. 3.

With high plastic deformation due to the reduction of the number of deformation passes, the reduction of dimple density in high-alloy samples even leads to a change in the nature of fractures to brittle and a sharp increase in the toughness at fracture from T = 0.11 GPa % for Zn-0.5 Mg to T = 0.18 GPa % and T = 1.8 GPa %, respectively, for Zn–1Mg and Zn-1.5 Mg alloys, Fig. 22. The relationship between Zn–1Mg and Zn-1.5 Mg increases 10-fold, which is connected with an almost 20-fold increase of $\varepsilon_u$ with the same $d_{eq}$ and comparable YS and $\varepsilon_f$, Fig. 22. Comparison for Zn-1.5 Mg alloy, Fig. 19d with Fig. 22b clearly indicates the positive effect of more deformation passes on the increase in strength and the corresponding decrease in T.

It should be noted that the micrometric Zn and UFG of Zn–Mg binary alloys after HE behave similarly to pure Al obtained by the combination of ECAP and annealing processes described in Ref. [34]. For both types of materials, the decrease in T corresponds to significant decreases, with grain increase, of yield stress YS, Fig. 23, and uniform elongation $\varepsilon_u$, Fig. 24. However, for the two lower alloys, Zn-0.5 Mg and Zn–1Mg, at close to and sub-micrometer grain sizes, there is a sharp decrease in $\varepsilon_u$, which was also reported for AA1050 by Yu et al. [36], despite the occurrence of plastic dimples, Fig. 19b–d. One explanation may be different characteristics of deformation of the fraction of smaller grains compared to larger ones and the distribution of the deformation structure, more uneven for smaller grains and more even for larger ones. The insert in Fig. 24 shows that the equalized values of the uniform deformation $0.9 < \varepsilon_u < 1.06$ for 4-pass HE of Zn–Mg binary alloys, regardless of the expressed differences in the strength of the materials, lead to slight differences in their toughness $0.34 < T < 0.41$, Fig. 19b–d, while for 2-pass HE of alloys, the drastic differences in uniform deformation $0.17 < \varepsilon_u < 5.6$ lead to large differences in toughness $0.11 < T < 1.89$, Fig. 22. This means a critical and directly proportional impact of $\varepsilon_u$ on the increase of T.

In addition to $d_{eq}$ and $\varepsilon_u$, the degree of uniformity of particle distribution of 2nd phase particles (eutectic) around the αZn grain on the cross-section of the tested rod is of particular importance for the value

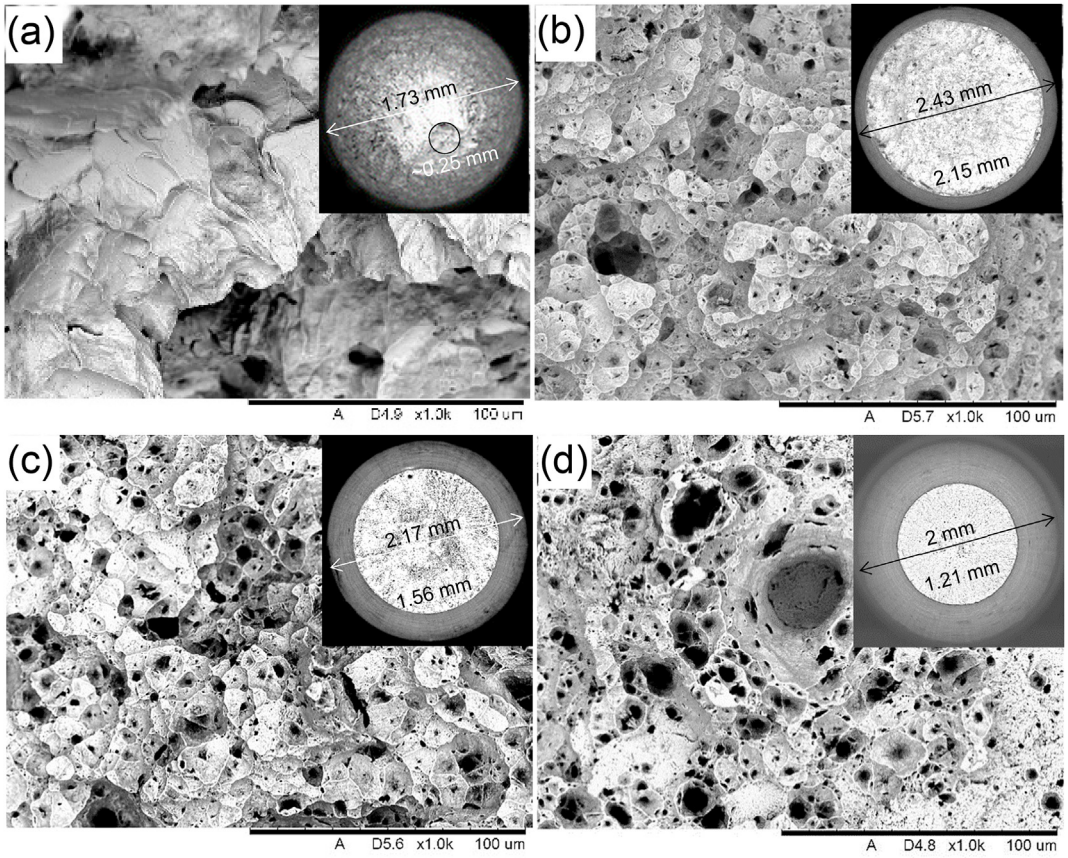


**Fig. 19.** Comparison of tensile fractures of (a) Zn, (b) Zn-0.5 Mg, (c) Zn–1Mg, and (d) Zn-1.5 Mg after room temperature cumulative hydrostatic extrusion in 4-passes with total true strain $\varepsilon_{cum}$ = 3.5; Note: insets show SEM images of torn cross section and sizes of thinning (*arrows*) and necking (*without arrows*) portions.

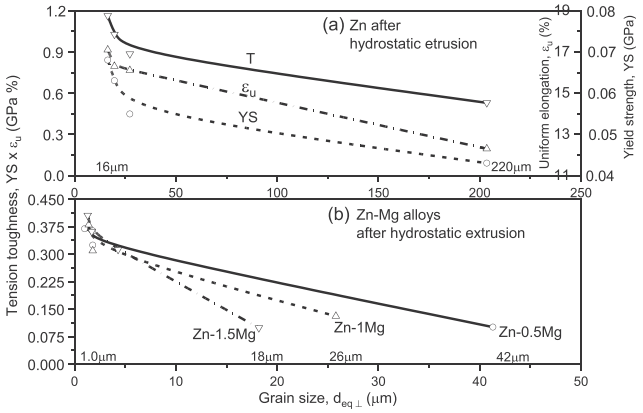


**Fig. 20.** Tension toughness vs. grain size variation for (a) Zn and (b) Zn–Mg binary alloys after hydrostatic extrusion.

of T, Fig. 25. Between alloys (a) Zn-0.5 Mg and (c) Zn-1.5 Mg there is an almost 20-fold difference in T, with a predominance for Zn-1.5 Mg, resulting from a more dense and even distribution of the stretched eutectic fibres and *α*Zn bands between them.

### 3.8. Tension toughness after cryo-deformation

Tension toughness T is more sensitive to cryo-deformation than to deformation at ambient temperature. Fig. 26 shows the tensile fractures of the Zn-0.5 Mg alloy after cryo-HE (a) in 4 passes, and (b) in 2 passes, with the same $\varepsilon_{cum}$ = 3.55. Fig. 26a corresponds to the fracture after HE at ambient temperature presented in Fig. 19b. Necking thickness reduction at cryo-HE is lower by ~50% for HE in 4 passes and higher by ~70% for more dynamic HE in 2 passes, which is due to higher strain hardening in the second case. Therefore, higher $\varepsilon_u$ of 4-pass samples 1.7, Fig. 26a, is observed, compared to 2-pass samples 0.24, Fig. 26b and, as a result, the much higher fracture work required due to a 6-fold higher toughness of a 4-pass cryo sample T = 0.51 GPa % compared to a 2-pass sample. In contrast, at ambient temperature, T is lower than at cryo conditions and amounts to T = 0.37 GPa %, and has been increased 3-fold compared to the 2-pass sample.

In summary, it should be concluded that in order to increase T, it is advantageous to carry out plastic deformation under conditions of more than one pass of deformation at ambient temperature or, in order to strengthen the effect, to carry it out additionally under cryogenic conditions. At the same time, a slight decrease in UTS is to be expected, compensated by higher YS and $\varepsilon_f$, in particular for more intensive cryo-HE in 2 passes. Replacement of the 1-pass cryo-HE with 2 passes increases the strength of UTS and YS by ~15%, HV does not change and significantly increases $\varepsilon_f$ plasticity by more than 65% at the expense of reducing $\varepsilon_u$, and thus reducing T by more than 60%. Each increase in the number of HE passes above two drastically increases T, which results from an increase in $\varepsilon_u$ work and a decrease in the AH effect resulting from mechanical extrusion work.

### 3.9. Tension toughness after combination of deformation processes

The highest T = 0.51 was obtained after 4 passes of cryo-HE and the next, lower by ~25% T = 0.39 after joining HE portions with ECAP at room temperature, Fig. 27, on which for the Zn-0.5 Mg alloy the homogeneity and size of dimples on fractured surfaces were presented. The tensile properties of $\varepsilon_f$, $\varepsilon_u$, YS and UTS (a) after cryo-HE were 16.3%, 1.7%, 301 MPa and 504 MPa, respectively, compared to (b) after ECAP + HE 10.6%, 1.39%, 278 MP and 420 MPa. This was

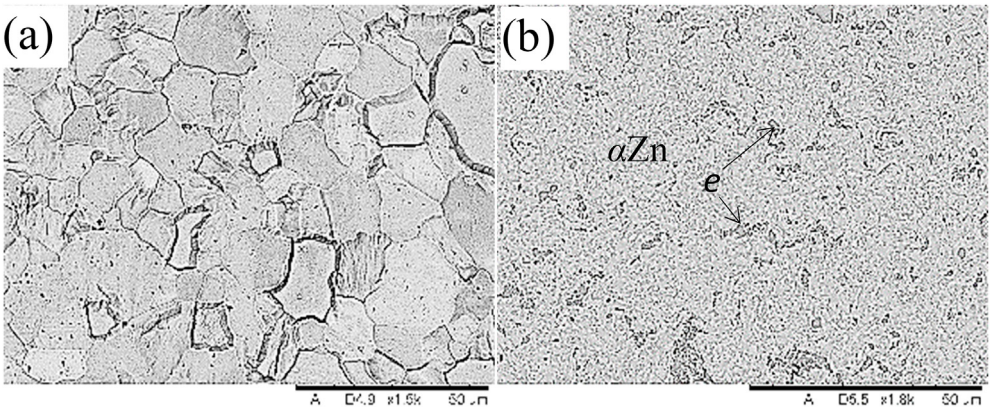


**Fig. 21.** SEM microstructures of transverse sections of (a) Zn, (b) Zn-0.5 Mg alloy after 4-passes hydrostatic extrusion with cumulative true strain $\varepsilon_{cum}$ = 3.55.

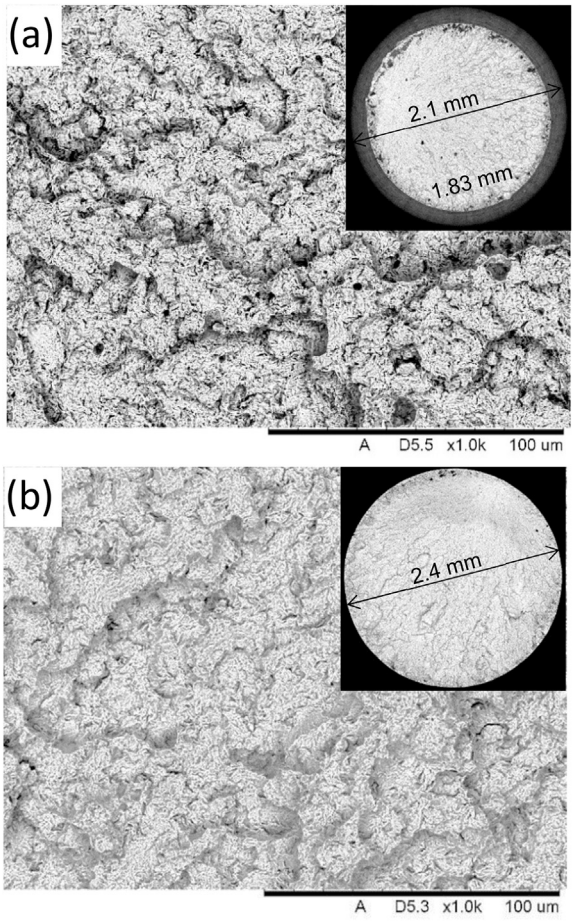


**Fig. 22.** Comparison of tensile fractures of (a) Zn–1Mg, and (b) Zn-1.5 Mg after room temperature cumulative hydrostatic extrusion in 2-passes with total true strain $\varepsilon_{cum}$ = 3.5; Note: insets show SEM images of torn cross sections and sizes of thinning (*arrows*) and necking (*without arrows*) portions.

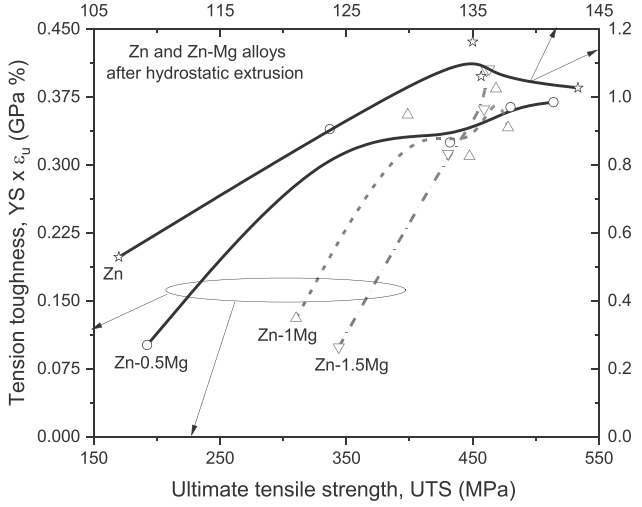


**Fig. 23.** Tension toughness T vs. ultimate tensile strength UTS for Zn and Zn–Mg binary alloys after hydrostatic extrusion.

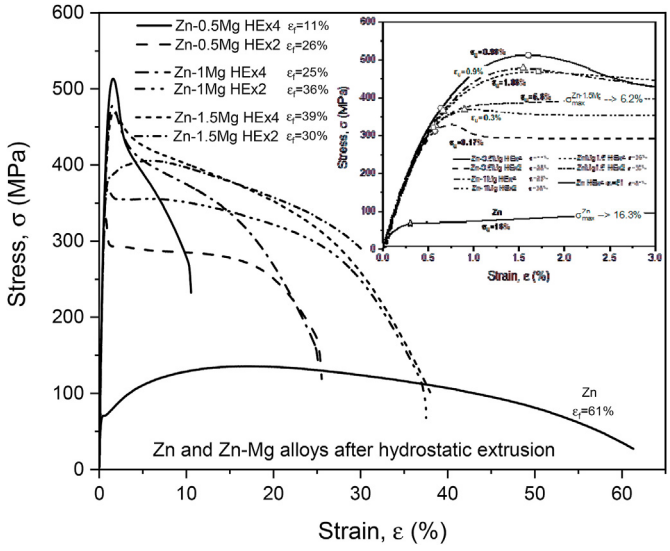


**Fig. 24.** Static uni-axial tensile characteristics for Zn and Zn-0.5 Mg, Zn–1Mg and Zn-1.5 Mg alloys after 4- and 2-passes room temperature hydrostatic extrusion with cumulative true strain $\varepsilon_{cum}$ = 3.55; Note: inset shows enlargement up to 3% elongation.

reflected in the homogenous distribution of finer dimples after cryo-deformation, Fig. 27a, and the heterogeneous, chaotic distribution of dimples of different sizes obtained by combining two processes with different deformation paths, Fig. 27b. This indicates the importance of the uniformity of distribution and refinement of dimples and high $\varepsilon_u$ and YS combined with high $\varepsilon_f$, and UTS for the value of T.

### *3.10. Severe plastic deformation during tensile test*

The fine-grained structure in Zn–Mg binary alloys may be conducive

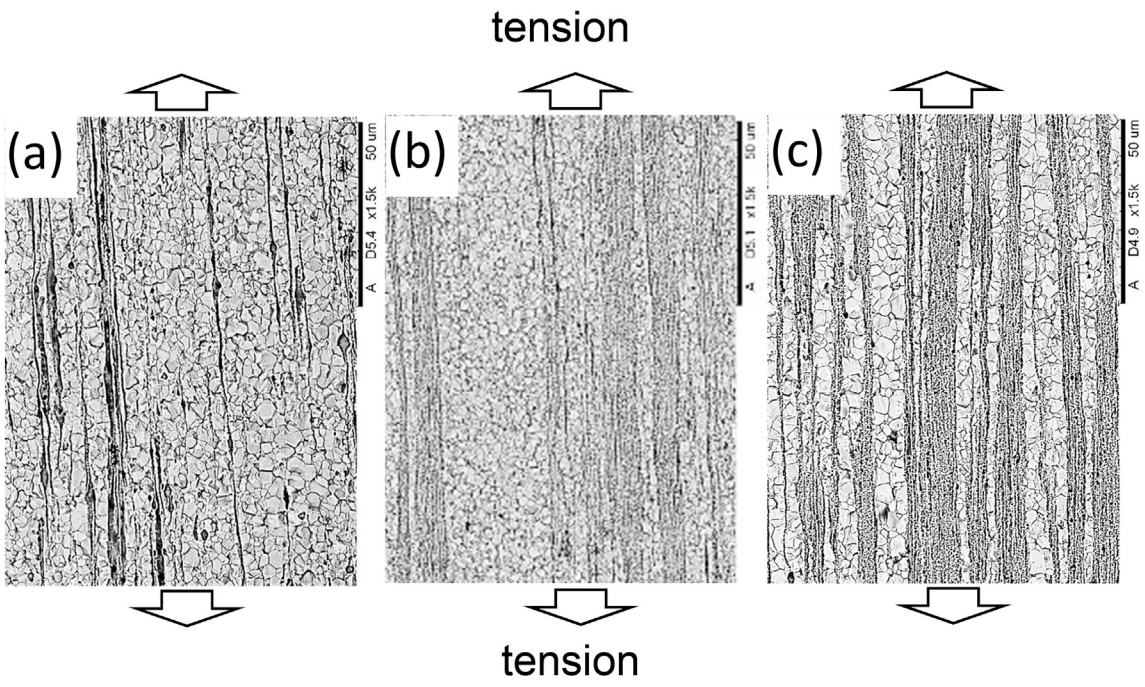


**Fig. 25.** Light microscopy longitudinal images of (a) Zn-0.5 Mg, tension toughness T = 0.1 GPa %, (b) Zn–1Mg, T = 0.2 GPa %, and (c) Zn-1.5 Mg, T = 1.8 GPa % alloys after 2-passes room temperature hydrostatic extrusion with cumulative true strain $\varepsilon_{cum}$ = 3.55.

to the achievement of the phenomenon of superplasticity in large deformations. Superplastic flow was observed in the Zn–Al–Ag alloy in the temperature range 373–523 K [37], and more recently in the Zn-0.5 Cu alloy at ambient temperature during multipass ECAP up to $\varepsilon_{cum}$ = 4.6 for mean size of dominant grains ~ 1 μm and a few grains exceeding 10 μm, leading to the highest $\varepsilon_f$ = 510% at $\dot{\varepsilon} = 1 \times 10^{-4}\ s^{-1}$ [38]. In this paper for the Zn-1.5 Mg alloy after HE, static tensile tests were carried out at ambient temperature with four $\dot{\varepsilon}$ of $8 \times 10^{-3}$, $10^{-3}$, $10^{-4}$ and $10^{-5}\ s^{-1}$, Fig. 28. As expected, decreasing $\dot{\varepsilon}$ resulted in a steady decrease in UTS, YS and $\varepsilon_u$ and an increase in $\varepsilon_f$. The highest $\varepsilon_f$ = 150% was achieved for $\dot{\varepsilon} = 10^{-5}\ s^{-1}$ which, however, according to Langdon's definition [39], does not meet the condition of superplastic flow, i.e. $\varepsilon_f$ above 400%. As mentioned above, the alloy Zn-1.5 Mg passes during HE at ambient temperature to $\varepsilon_{cum}$ = 3.55–10 times the grain size refinement, from 18 to 1.4 μm, Fig. 10b, which is the initial material for tensile tests. At the lowest $\dot{\varepsilon} = 10^{-5}\ s^{-1}$, a slight grain size increase and elongation in the tensile direction is observed, and at the standard $\dot{\varepsilon} = 8 \times 10^{-3}\ s^{-1}$, due to the process carried out under much higher stress, a higher degree of hardening and refinement of the grains in comparison with the initial material, Fig. 28.

Fig. 29 shows the relationship between flow strain and $\varepsilon_f$ as a function of $\dot{\varepsilon}$ for the Zn-1.5 Mg alloy for tensile tests at ambient temperature. The flow stress was defined as the value of the true stress at 10% elongation. In the low stress area and the lowest $\dot{\varepsilon}$, the parameter of sensitivity to the deformation rate m ~0.27 slightly exceeds that obtained for similar $\dot{\varepsilon}$ for the Zn-0.5 Cu alloy after ECAP [39]. This may be due to the higher density of second phase inclusions located at grain boundaries and their interaction with dislocations for 1.5% of the Zn-1.5 Mg alloy compared to 0.5% of the Zn-0.5 Cu alloy. On the other hand, the area with medium stress and high $\varepsilon_f$ is characterized by a reduction of the parameter by half to m ~0.12, Fig. 29a, which may be caused by strain-generated grain growth during the tensile test. However, the more important factor seems to be the heterogeneity of the microstructure in the initial material prior to fracture, which at higher $\dot{\varepsilon}$ causes heterogeneous deformation during fracture. The arithmetic mean of Zn-1.5 Mg alloy grain size after HE on the cross-section for all

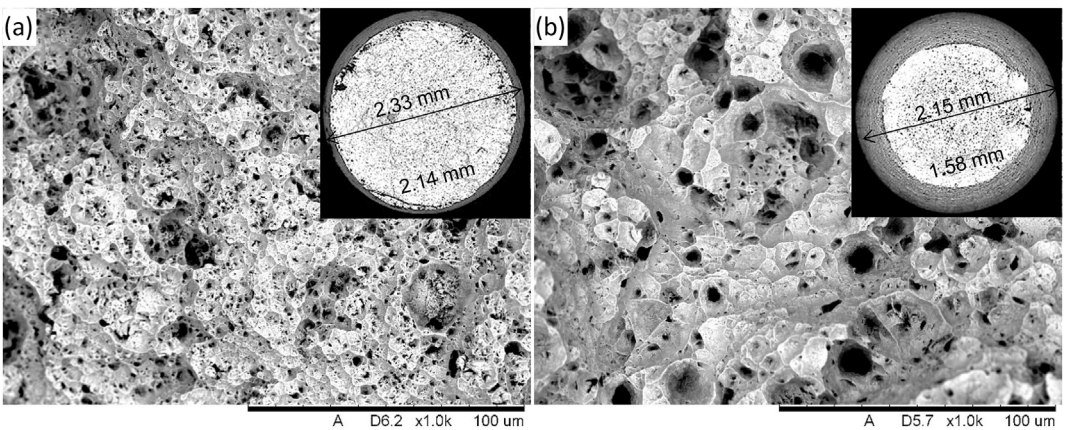


**Fig. 26.** Comparison of tensile fractures of Zn-0.5 Mg after cryo-hydrostatic extrusion (a) in 4-passes, and (b) in 2-passes, both with total true strain $\varepsilon_{cum}$ = 3.55, both exhibiting ductile mode of fracture with much smaller dimples in the first case. As a result (a) shows almost twice smaller elongation to fracture $\varepsilon_f$ = 16% vs. 30%, smaller yield stress YS = 300 MPa vs. 340 MPa and higher grain size 3.1 μm vs. 1.9 μm.

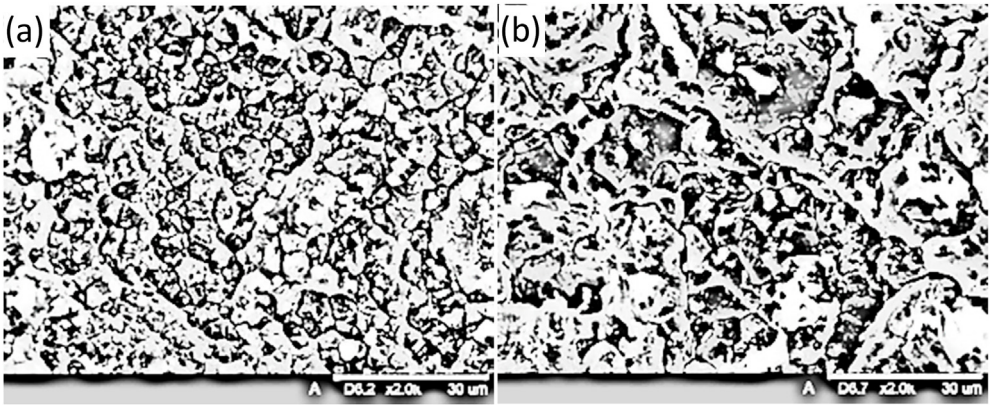


**Fig. 27.** Comparison of dimple sizes after uniaxial tensile tests of Zn-0.5 Mg alloy rods made by: (a) cryo-hydrostatic extrusion HE in 4-passes with $\varepsilon_{cum}$ = 3.52, tensile toughness T = 0.51 GPa %, and (b) combination of 2-passes of ECAP followed by 2 passes of room temperature HE, $\varepsilon_{cum}$ = 3.22, T = 0.39 GPa %.

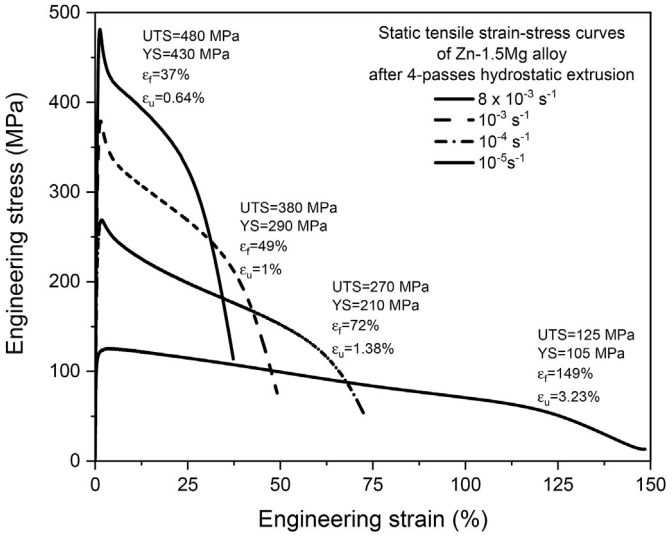


**Fig. 28.** Engineering stress-strain curves dependence on the true strain rate of Zn-1.5 Mg alloy after 4-pass room temperature hydrostatic extrusion with cumulative true strain $\varepsilon_{cum}$ = 3.55.

grains was 0.8 μm and the mean value only for large grains $\alpha$Zn 1.4 μm, both with similar standard deviation SD(d) = 0.5 μm, which gives a CV (d) coefficient of variation of ~0.63 and ~0.35, respectively. Similar figures were obtained for the longitudinal cross-section. The unstable size of smaller grains, including those contained in 2-phase $\alpha$Zn + $Mg_2Zn_{11}$ eutectic, may be responsible for the structural heterogeneity generated and developed during the fracture, and the resulting constant decrease of $\varepsilon_u$, Figs. 5 and 6, and thus a decrease in deformation to fracture $\varepsilon_f$, Fig. 29b.

One important factor in biodegradable stents is the relatively high m determining $\dot{\varepsilon}$ of the material and avoiding the strain localized in the stent, as the stent undergoes a significant ε during expansion. The value of m = 0.27 for Zn-1.5 Mg is within the acceptable limits of the stent material if it expands slowly enough, Fig. 29.

### 3.11. Uniaxial compression

It has long been observed for the Zn–1Mg alloy that the stress-strain curves for compression show a superaplastic character, which is attributed to the formation of the compressive twin grains [40]. For this reason, the compression process does not allow the maximum ultimate compressive strength ($\sigma_M$) to be determined unambiguously, but only the compressive yield strength ($\sigma_{0.2}$). Compressive strength can only be determined for the assumed degree of compression strain, which for the compression range ε = 80% is shown in Fig. 30. What is understandable, the $\sigma_M$ increases with the increase in alloying, and for Zn and subsequent Zn–Mg binary alloys it is 723, 1573, 1803 and 2195 MPa, respectively. For 80% deformation, none of the materials cracked, and the uni-axial compression processes could continue without failure, meaning that the actual $\sigma_M$ values are higher than those given above. The compressive yield strength $\sigma_{0.2}$ as a function of ε increased the strongest for Zn-0.5 Mg (by more than 230% to 473 MPa), average for Zn–1Mg (by 55%–446 MPa), and the weakest for Zn-1.5 Mg (by 12%–425 MPa), Fig. 31. For Zn, the $\sigma_{0.2}$ value did not change. For alloy Zn–1Mg after cryo-HE, compared to HE at ambient temperature, $\sigma_{0.2}$ was lower than 5%–20%, while $\sigma_M$ was minimally higher.

In Ref. [5] for cast and rolled- or hot-extruded Zn–1Mg alloy an increase $\sigma_{0.2}$ was presented to 285 MPa, attributing this to the effect of the alloying additive Mg. This was confirmed by tests of Mostaed et al. [7], in which materials extruded at 250 °C showed $\sigma_{0.2}$ for Zn 74 MPa, Zn-0.5 Mg 260 MPa and Zn–1Mg 320 MPa with a grain diameter between 4 and 4.5 μm. However, such properties are insufficient for the surface of many biodegradable elements carrying high bearing loads, typically requiring the strength of > 300 MPa and $\varepsilon_f$ > 15% [41,42]. Ongoing studies have presented that in order to achieve such values, two main conditions must be met: (i) increase in ε of the Zn–Mg binary alloys, and (ii) reduction of the temperature at which their plastic deformation is carried out.

### 3.12. Hardness and compressive strength after immersion test

Zn–Mg binary alloys intended for implants must have sufficient strength for as long as the damaged tissue is not healed, sometimes causing long exposure to human body fluids. The effect of the corrosion effect on the mechanical properties of round rods made of Zn–Mg binary alloys after HE were tested on the basis of changes in dimensions of short, cylindrical samples and their hardness and strength at uniaxial compression before and after being subjected to immersion tests in modified Hank solution for up to 180 days. Corrosive immersion tests and their analysis were conducted by A. Jarzębska [43] as part of her doctoral dissertation. For samples without the corrosion test, HV increases with Mg from 32 HV0.2 for Zn, through 106 HV0.2 for Zn-0.5 Mg to ~115 HV0.2 for both Zn–1Mg and Zn-1.5 Mg alloys, Fig. 32. After the immersion test, with the exception of Zn, the HV of all Zn–Mg binary alloys decreases with test time at different rates. After 90 days of immersion, the HV decreased with an increase of Mg alloy addition by 40%, ~13%–~10% respectively. After exceeding 90 days of immersion, the hardness degradation of Zn–1Mg and Zn-1.5 Mg alloys accelerated significantly to 180 days lower than the initial state, by 65% and 35% respectively. However, in the period of 90–180 days the alloy Zn-0.5 Mg showed a slight increase in HV, approaching a level comparable

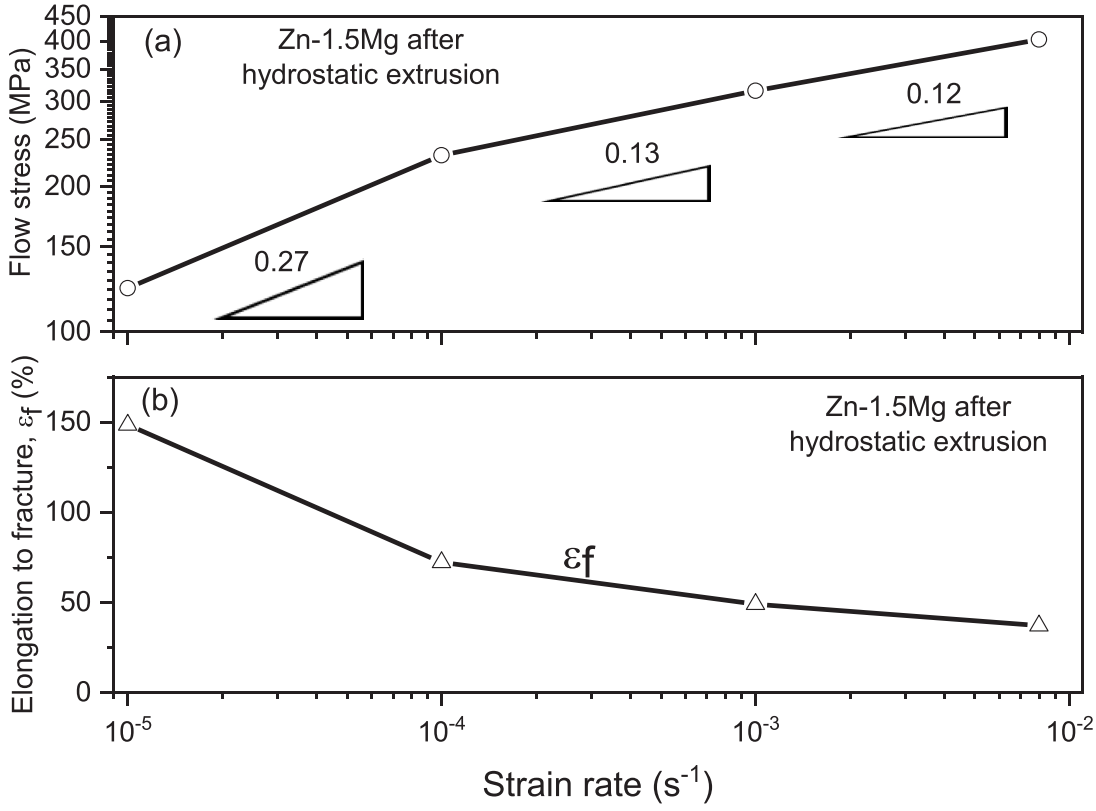


**Fig. 29.** Variation of (a) flow stress, and (b) elongation to fracture with strain rate at 295 K of Zn-1.5 Mg alloy processed by 4-pass room temperature hydrostatic extrusion with cumulative true strain $\varepsilon_{cum}$ = 3.55.

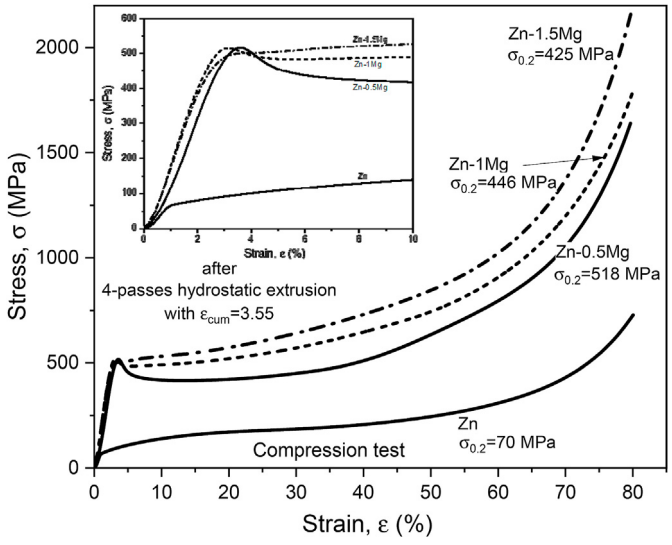


**Fig. 30.** Stress-strain curves at compression test of 4-pass room temperature hydrostatically extruded Zn and Zn–Mg binary alloys with cumulative true strain $\varepsilon_{cum}$ = 3.55.

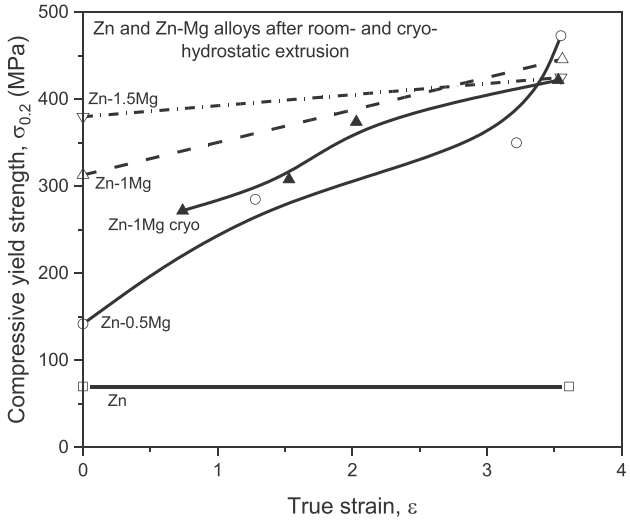


**Fig. 31.** Variation of compressive yield strength $\sigma_{0.2}$ with true strain ε after room temperature and cryo-hydrostatic extrusion of Zn and Zn–Mg binary alloys.

to Zn-1.5 Mg, i.e. ~35%.

The lower degradation rate of HV with an increase in Mg alloy addition may indicate an increase in the uniformity of particle distribution of the second phase of $Mg_2Zn_{11}$ with an increase in their volumetric share in the alloy, which confirms the basic advantage of the cold HE process, which is the homogeneous distribution of volumetric deformation at high strains, unattainable with classical deformation processes such as conventional extrusion, rolling, etc. This is confirmed by the results of uni-axial compression of the HE samples presented in Table 1. It should be noted that Zn–Mg HE samples after 10 and 30 days of immersion showed an increase of $\sigma_{0.2}$, which additionally increased with an increase in Mg, as opposed to the samples after conventional extrusion at 250 °C, for which the whole range of Zn–Mg binary alloys from 0.15% to 3.0% showed degradation of yield strength at compression already after 14 days of the immersion test [7]. This was attributed to particle increase of the second phase of $Mg_2Zn_{11}$ and its

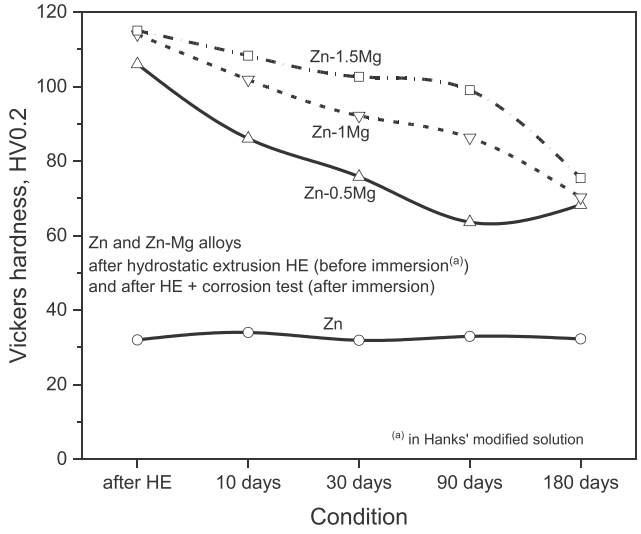


**Fig. 32.** Vickers hardness HV0.2 of the samples at room temperature before and after immersion in Hanks' modified solution after 4-pass room temperature hydrostatic extrusion of Zn and Zn–Mg binary alloys with cumulative true strain $\varepsilon_{cum} = 3.55$.

**Table 1**
Compressive yield strength $\sigma_{0.2}$ increase (+) or reduction (−) after immersion in Hanks' modified solution.

| Sample | 10 days (%) | 30 days (%) | 14 days [a](%) |
|---|---|---|---|
| Zn | −2.0 | −5.2 | −8.7 |
| Zn-0.5 Mg | +10.2 | +6.3 | −14.2 |
| Zn–1Mg | +12.6 | +11.9 | −19.7 |

[a] Ref. [7].

uneven distribution, which led to strong localized galvanic corrosion and hence a decrease in mechanical cohesion after the immersion test. Strong structural heterogeneity and related decreases of $\sigma_{0.2}$ resulted from a more coarse structure $d_{eq} > 4.1–4.4$ μm and high structural heterogeneity due to lower hot plastic deformation $\varepsilon = 1.8$ [7], compared to material after HE deformed at ambient temperature with 2 times higher $\varepsilon_{cum} = 3.6$ leading to more than 3 times lower $d_{eq} = 1–1.4$ μm and significantly higher structural homogeneity, which for the 180-day immersion test is presented in Fig. 32. For Zn, regardless of the length of the immersion test, a reduction of $\sigma_{0.2}$ was observed. However, it was 40% lower for the material after HE compared to the material after conventional extrusion in 250 °C despite the twice shorter immersion test [7], Table 1. This can be attributed to an almost 10 times higher microstructure refinement of 16.4 μm vs. 151 μm in the first case.

Such a significant reduction in yield stress in Zn and Zn–Mg binary alloys was made possible by conducting forming under high pressure to promote mechanical integration of the initial material prior to uni-axial pressing and immersion testing. A good combination of mechanical properties with no corrosive plasticity degradation makes Zn-0.5 Mg and Zn–1Mg alloys good candidates for biodegradable implants, e.g. vascular stents.

### 3.13. Comparison of Zn–Mg binary alloys processed by HE with other techniques

Table 2 presents a comparison of mechanical properties determined by static tensile and compression methods for Zn and Zn–Mg binary alloys studied in this paper with literature data. The results indicate that the highest property values are obtained by using the HE process at ambient temperature. This is influenced by basic factors which are closely related to each other: (i) strong refinement of the microstructure to ~ 1 μm due to large plastic deformation reaching $\varepsilon_{cum} = 3.55$ (97% percentage deformation), and (ii) the possibility of generating a large ε at ambient temperature due to the application of deformation in several passes, which limits the AH effect generated during plastic deformation inhibiting the increase of the grain growth by limiting the healing and recrystallisation processes. None of the other deformation processes commonly used for Zn and Zn–Mg binary alloys, i.e. hot rolling and extrusion, exceed $\varepsilon = 3$, instead oscillating closer to or below $\varepsilon = 2$. As Table 2 shows, the HE process at ambient temperature allows for a 3 to 4-fold reduction in grain size compared to the next best commonly used

**Table 2**
Mechanical properties of biodegradable zinc alloys.

| Metal/Alloy | Processing | Temperature (°C) | Average grain size $d_{eq}$ (μm) | Yield strength *YS* (MPa) | Ultimate tensile strength *UTS* (MPa) | Elongation (%) | Compressive strength $\sigma_{0.2}$ (MPa) | Hardness *HV* | Ref. |
|---|---|---|---|---|---|---|---|---|---|
| Zn | As cast | | > 500 | 10 | 18 | 0.32 | | 38 | [5,6] |
| | Hot rolling | 250 | | 30 | 50 | 5.8 | | 40 | [6] |
| | Hot extrusion | 210 | | 37 | 62 | 3.5 | 103 | | [6] |
| | HPT[a] room | | 80 | | ~150 | ~25 | | 35 | [44] |
| | Hot extrusion | 250 | 151 | 51 | 111 | 60 | 77 | 34 | [7] |
| | **HE[b] room** | | **16.4** | **68** | **135** | **61.2** | **70** | **32** | **present** |
| Zn-0.02 Mg | Hot extr. + WD[c] | 200 | 1.1 | 388 | 455 | 5.4 | | | [14] |
| Zn-0.08 Mg | Hot extr. + WD | 150 | 6.3 | 220 | 340 | 40 | | 103 | [13] |
| Zn-0.5 Mg | Hot extrusion | | 4.1 | 159 | 297 | 13 | 258 | 65 | [6] |
| | **HE room** | | **1.0** | **373** | **514** | **10.5** | **473** | **107** | **present** |
| Zn-0.8 Mg | Hot rolling | 250 | | 260 | 268 | 7.2 | | | [12] |
| Zn–1Mg | As cast | | 50–100 | 95 | 140 | 1.66 | | | [48] |
| | As cast | | | 128 | 185 | 1.82 | | 78 | [5] |
| | Hot rolling | 250 | | 253 | | | | | [5] |
| | Hot extrusion | 200 | < 10 | 180 | 252 | 12 | | | [48] |
| | Hot extrusion | 210 | 4.4 | 180 | 340 | 6 | 320 | 75 | [7] |
| | **HE room** | | **1.4** | **367** | **478** | **24.9** | **453** | **111** | **present** |
| Zn-1.5 Mg | As cast | | | 112 | 151 | 1.25 | | 155 | [49] |
| | **HE room** | | **1.4** | **356** | **463** | **38.6** | **425** | **120** | **present** |
| Zn–3Mg | Homogenisation | 360/15h | | | 88 | 8.8 | | 175 | [20] |
| | As cast | | | | 104 | 2.3 | | 201 | [20] |
| | Hot extrusion | | | 291 | 399 | 1 | 497 | 117 | [7] |

[a] HPT – high pressure torsion.
[b] HE – hydrostatic extrusion.
[c] WD - wire drawing.

process, i.e. hot extrusion [7]. The only process other than the HE process conducted at ambient temperature, i.e. the high pressure torsion HPT process for Zn [44], in which the true strain exceeds $\varepsilon > 5$, leads to a relatively high UTS = 150 MPa. However, samples in the form of 10 mm × 0.9 mm discs are not suitable as prefabricates for the production of vascular stents.

Achieving high deformation at ambient temperature in the HE process is possible by running the process under high hydrostatic pressure and the interaction of 3-axial compressive stress on the deformation zone which inhibits the processes of material disintegration through the generation and propagation of cracks. The efficiency of grain refinement in the HE process has been repeatedly reported for pure metals and alloys, such as titanium [45], magnesium alloys [46] and copper alloys [27]. The grains are strongly refined after HE and help to stop the drop in plasticity due to the easier adaptation of the grains to slip and rotation. In addition, the increased number of grain boundaries favours a significant increase in strength due to the formation of a significant number of barriers to dislocation movement [47].

The lowest benefits compared to hot extrusion are achieved with the HE process at ambient temperature, with respect to Zn, resulting in increases of YS, UTS and $\varepsilon_f$ of more than 30%, more than 20%, and 2%, respectively. At the same time, there is a decrease of $\sigma_{0.2}$ by 9% and HV by 6%. The changes of YS, UTS, $\varepsilon_f$, $\sigma_{0.2}$ and HV after HE compared to hot extrusion are, respectively, for the Zn-0.5 Mg binary alloy: 135%, 73%, −19%, 83% and 65%, and for Zn–1Mg binary alloy: 104%, 41%, 315%, 42% and 48%. Comparison of Zn-1.5 Mg binary alloy after HE with the alloy in the casting state gives YS, UTS and $\varepsilon_f$ increases by 218%, 207% and 2988%, respectively, and HV decreases by 23%.

Recently, to satisfy the property requirements for biodegradable medical implants, research on low-Mg alloyed Zn binary alloys was intensified, as for 0.1 to 0.8 wt% of Mg [12], 0.02 wt% of Mg [14] and even as low as 0.08, 0.005 and 0.002 wt% of Mg [13], Table 2. For Zn-0.8 Mg binary alloy hot-rolled at 250 °C to 1 mm in thickness the positive role of the refined $Mg_2Zn_{11}$ intermetallic phase and fine grain size in inhibiting of twinning was observed resulting in better strength and ductility in comparison to the as-cast material but not enough strong for stent applications [12]. In Zn-0.02 Mg binary alloy hot extruded at 200 °C and multi-pass wire drawn at room temperature to diameter of 0.8 mm carried out at a speed of 40 mm $s^{-1}$ the dynamic recrystallisation occurred leading despite this to high strength 455 MPa but insufficient ductility 5.4% [14]. It was a result of complex, competitive action of work hardening, recrystallisation softening and grain boundary strengthening contributed to the mechanical properties evolution. In Zn-0.08 Mg binary alloy hot-extruded at 150 °C and drawn at room temperature into wire of 0.25 mm in diameter the best integration of strength 340 MPa and ductility 40% was obtained, attributed universally to finer grains and an increased amount of hard $Mg_2Zn_{11}$ intermetallic phases [13]. The common features of the last two cases include: (i) decrease of the Mg alloying element, (ii) reduction of the cross sections of fabricated wires, and (iii) introduction as the last step the plastic deformation at room temperature. Unfortunately, for low alloyed materials the thin dimension of cross sections combined with high strain rates promote efficient thermal softening and inhibit grain refinement which eliminates material as the reliable candidate for vascular stent applications.

Process HE at ambient temperature allows the production, from Zn and Zn–Mg binary alloys of several metres-long sections of bulky solid rods with high mechanical properties. This technology allows for strength enhancement of about 2 times for Zn-0.5 Mg and Zn–1Mg alloys, and about 3 times for the Zn-1.5 Mg alloy in comparison with materials produced by other methods. This creates good prospects for medical applications of these materials in the manufacture of high-strength biodegradable implants, such as vascular stents.

## 4. Summary and conclusions

Cumulative hydrostatic extrusion HE of hypoeutectic Zn–Mg binary alloys produces a fine-grained structure composed of a mixture of αZn and αZn + $Mg_2Zn_{11}$ eutectic segregated at grain boundaries. The HE process, compared to the commonly used hot forming processes for Zn–Mg binary alloys, allows for 3 to 4 times greater grain size reduction to ~1.0 μm. In order to achieve high hardness and strength, the HE process should be carried out cumulatively in at least 4 passes to cumulative true strain $\varepsilon_{cum}$ ~3.55. The highest strength and yield strength UTS = 515 MPa and YS = 375 MPa were obtained for Zn-0.5 Mg alloy and the highest percentage elongation to fracture $\varepsilon_f$ over 38% and microhardness 120 HV0.2 for Zn-1.5 Mg alloy. In order to give Zn–Mg binary alloys a high load-bearing capacity it is necessary to maintain two basic conditions during their production: (i) to generate high plastic deformation, and (ii) to minimise the temperature at which it is produced. The structural homogeneity after HE promotes an increase in the compression yield strength $\sigma_{0.2}$.

The HE process activates a strong adiabatic heating effect increasing with Mg content in the $T/T_m$ range 0.5–0.54 for Zn and 0.6–0.85 for Zn–Mg binary alloys. This effect can be reduced by cumulative extrusion and by cooling the extruded rod at the exit from the die, which reduces the effects of recrystallisation and increases the structure refinement. The HE from the temperature of liquid nitrogen $LN_2$, results in higher texturisation of the αZn + $Mg_2Zn_{11}$ eutectic and stronger grain refinement maintaining a higher density of structural defects, which causes a 50% increase in hardness compared to deformation at room temperature. The combination of the ECAP process preceding the cumulative HE leads to an improvement in grain texture and grain refinement, which is the result of a change in the deformation path and a synergistic effect of greater refinement and homogenisation of the microstructure, increasing the mechanical and plastic properties of Zn–Mg binary alloys.

The homogeneity of dimple distribution at fracture is more important for toughness than their size, resulting in high uniform elongation $\varepsilon_u$ and high yield strength YS combined with high strength UTS. For Zn-1.5 Mg binary alloy, lowering the number of HE passes to two raises the toughness to the highest measured value of 1.8 GPa %, resulting in a drastic increase of $\varepsilon_u$ to 5.6%. This confirms the critical and directly proportional effect of $\varepsilon_u$ on the increase of toughness at fracture. Decreasing the deformation speed at fracture to $10^{-5}$ $s^{-1}$ for the Zn-1.5 Mg binary alloy causes an increase in $\varepsilon_f$ to a maximum of 150%, which does not meet the superplasticity condition. The sensitivity to the deformation rate m for Zn-1.5 Mg binary alloy after HE at ambient temperature is 0.27 and is within acceptable limits for materials used to produce stents. The corrosion rate for Zn–Mg binary alloys after HE decreases, with an increase in the alloying additive Mg, and is significantly lower compared to alloys obtained by classical hot forming methods. This confirms the homogeneous volumetric distribution of the degree of plastic deformation when using the hydrostatic extrusion method.

The highest fracture and compression properties, compared to literature data, for Zn and its alloys are obtained by using the HE process at ambient temperature. This is due to two interrelated factors: (i) the generation of severe plastic deformations at ambient temperature, and (ii) refinement of the microstructure to ~ 1 μm due to deformation under high hydrostatic pressure. The HE process enables the production of several-metre-long rods and wires, with a yield strength about 2 times higher for the Zn-0.5 Mg and Zn–1Mg binary alloys, and about 3 times higher for the Zn-1.5 Mg binary alloy in comparison with materials obtained by other methods. Zn–Mg binary alloys have mechanical and corrosive characteristics qualifying them for medical applications in the form of high-strength biodegradable implants, e.g. for vascular stents.

## CRediT authorship contribution statement

**W. Pachla:** Conceptualization, Methodology, Writing - original draft, Data curation. **S. Przybysz:** Investigation, Formal analysis. **A. Jarzębska:** Investigation, Formal analysis. **M. Bieda:** Investigation. **K. Sztwiertnia:** Investigation. **M. Kulczyk:** Formal analysis, Data curation. **J. Skiba:** Investigation, Validation.

## Declaration of competing interest

The authors declare no conflict of interest.

## Acknowledgement

This work was financially supported by the National Science Centre (Poland), grant UMO-2016/23/B/ST8/00724.

## References

[1] H. Li, Y. Zheng, L. Qin, Progress of biodegradable metals, Prog. Nat. Sci. Mater. 24 (2014) 414–422.
[2] G. Katarivas Levy, J. Goldman, E. Aghion, The prospects of zinc as a structural material for biodegradable implants-A Review Paper, Metals 7 (2017) 1–18 402.
[3] N.S. Murni, M.S. Dambatta, S.K. Yeap, G.R.A. Froemming, H. Hermawan, Cytotoxicity evaluation of biodegradable Zn–3Mg alloy toward normal human osteoblast cells, Mater. Sci. Eng. C 49 (2015) 560–566.
[4] J. Kubasek, D. Vojtech, Zn-based Alloys as an Alternative Biodegradable Materials, Metal vols. 23–25, EU, Brno, Czech Republic, 2012 05.2012.
[5] H.F. Li, X.H. Xie, Y.F. Zheng, Y. Cong, F.Y. Zhou, K.J. Qiu, X. Wang, S.H. Chen, L. Huang, L. Tian, L. Qin, Development of biodegradable Zn-1X binary alloys with nutrient alloying elements Mg, Ca and Sr, Sci. Rep. 5 (2015) 1–13.
[6] H. Li, H. Yang, Y. Zheng, F. Zhou, K. Qiu, X. Wang, Design and characterizations of novel biodegradable ternary Zn-based alloys with IIA nutrient alloying elements Mg, Ca and Sr, Mater. Des. 83 (2015) 95–102.
[7] E. Mostaed, M. Sikora-Jasinska, A. Mostaed, S. Loffredo, A.G. Demir, B. Previtali, D. Mantovani, R. Beanland, M. Vedani, Novel Zn-based alloys for biodegradable stent applications: design, development and in vitro degradation, J. Mech. Behav. Biomed. Mater. 60 (2016) 581–602.
[8] M.P. Staiger, A.M. Pietak, J. Huadmai, G. Dias, Magnesium and its alloys as orthopedic biomaterials: a review, Biomaterials 27 (2006) 1728–1734.
[9] F. Witte, N. Hort, C. Vogt, S. Cohen, K.U. Kainer, R. Willumeit, F. Feyerabend, Degradable biomaterials based on magnesium corrosion, Curr. Opin. Solid State Mater. Sci. 12 (2008) 63–72.
[10] D. Vojtech, J. Kubasek, J. Serak, P. Novak, Mechanical and corrosion properties of newly developed biodegradable Zn-based alloys for bone fixation, Acta Biomater. 7 (2011) 3515–3522.
[11] X. Wang, H.M. Lu, X.L. Li, L. Li, Y.F. Zheng, Effect of cooling rate and composition on microstructures and properties of Zn–Mg alloys, Trans. Nonferrous Metals Soc. China 17 (Part A) (2007) 122–125.
[12] S. Liu, D. Kent, N. Doan, M. Dargusch, G. Wang, Effects of deformation twinning on the mechanical properties of biodegradable Zn-Mg binary alloys, Bioact. Mater. 4 (2019) 8–16.
[13] H. Jin, S. Zhao, R. Guillory, P.K. Bowen, Z. Yin, A. Griebel, J. Schaffer, E.J. Earley, J. Goldman, J.W. Drelich, Novel high-strength, low-alloys Zn-Mg (< 0.1 wt% Mg) and their arterial biodegradation, Mater. Sci. Eng. C 84 (2018) 67–79.
[14] L. Wang, Y. He, H. Zhao, H. Xie, S. Li, Y. Ren, G. Qin, Effect of cumulative strain on the microstructural and mechanical properties of Zn-0.02 wt%Mg alloy wires during room-temperature drawing process, J. Alloys Compd. 740 (2018) 949–957.
[15] S. Champagne, E. Mostaed, F. Safizadeh, E. Ghali, M. Vedani, H. Hermawan, In vitro degradation of absorbable zinc alloys in artificial urine, Materials 12 (2019), https://doi.org/10.3390/ma12020295 295.
[16] S. Dobrita, B. Istrate, N. Cimpoeşu, S. Stanciu, V. Apostol, R. Cimpoeşu, I. Ioniță, P. Paraschiv, Preliminary results on the corrosion behaviour of a new biodegradable metallic material based on zinc 374, IOP Conf. Ser. Mater. Sci. Eng. 374 (2018) 012027.
[17] Z. Liu, A new approach toward designing and synthesizing the microalloying Zn biodegradable alloys with improved mechanical properties, Metall. Mater. Trans. A 50A (2019) 311–325.
[18] J. Venezuela, M.S. Dargusch, The influence of alloying and fabrication techniques on the mechanical properties, biodegradability and biocompatibility of zinc: a comprehensive review, Acta Biomater. 87 (2019) 1–40.
[19] Zhang-Zhi Shi, Xi-Xian Gao, Hai-Jun Zhang, Xue-Feng Liu, Hui-Yan Li, Chao Zhou, Yu-Xia Yin, Lu-Ning Wang, Design biodegradable Zn alloys: second phases and their significant influences on alloy properties, Bioact. Mater. 5 (2020) 210–218.
[20] M.S. Dambatta, S. Izman, D. Kurniawan, S. Farahany, B. Yahaya, H. Hermawan, Influence of thermal treatment on microstructure, mechanical and degradation properties of Zn–3Mg alloy as potential biodegradable implant material, Mater. Des. 85 (2015) 431–437.
[21] X.B. Liu, D.Y. Shan, Y.W. Song, E.H. Han, Effects of heat treatment on corrosion behaviors of Mg–3Zn magnesium alloy, Trans. Nonferrous Metals Soc. China 20 (2010) 1345–1350.
[22] C.C. Kammerer, S. Behdad, L. Zhou, F. Betancor, M. Gonzalez, B. Boesl, Y.H. Sohn, Diffusion kinetics, mechanical properties, and crystallographic characterization of intermetallic compounds in the Mg-Zn binary system, Intermetallics 67 (2015) 145–155.
[23] H.Ll.D. Pugh, Mechanical Behaviour of Materials under Pressure, Elsevier Publ. Co. Ltd., 1970 Amsterdam.
[24] A.I. Ryazanov, S.A. Pavlov, M. Kiritani, Effective temperature rise during propagation of shock wave and high-speed deformation in metals, Mater. Sci. Eng. A 350 (2003) 245–250.
[25] F.K. Yan, G.Z. Liu, N.R. Tao, K. Lu, Strength and ductility of 316L austenitic stainless steel strengthened by nano-scale twin bundles, Acta Mater. 60 (2012) 1059–1071.
[26] M. Kulczyk, W. Pachla, A. Mazur, M. Suś-Ryszkowska, N. Krasilnikov, K.J. Kurzydłowski, Producing bulk nanocrystalline materials by combined hydrostatic extrusion and equal-channel angular pressing, Mater. Sci. Pol. 25 (4) (2007) 991–999.
[27] M. Kulczyk, W. Pachla, J. Godek, J. Smalc-Koziorowska, J. Skiba, S. Przybysz, M. Wróblewska, M. Przybysz, Improved compromise between the electrical conductivity and hardness of the thermo-mechanically treated CuCrZr alloy, Mater. Sci. Eng. A 724 (2018) 45–52.
[28] K.M. Youssef, R.O. Scattergood, K.L. Murty, C.C. Koch, Nanocrystalline Al–Mg alloy with ultrahigh strength and good ductility, Scripta Mater. 54 (2006) 251–256.
[29] D.C.C. Magalhaes, M.F. Hupalo, O.M. Cintho, Natural aging behavior of AA7050 Al alloy after cryogenic rolling, Mater. Sci. Eng. A 593 (2014) 1–7.
[30] P.N. Rao, D. Singh, R. Jayaganthan, Mechanical properties and microstructural evolution of Al 6061 alloy processed by multidirectional forging at liquid nitrogen temperature, Mater, Design 56 (2014) 97–104.
[31] N. Nayan, S.V.S. Narayana Murty, A.K. Jha, B. Pant, S.C. Sharma, K.M. George, G.V.S. Sastry, Mechanical properties of aluminium–copper–lithium alloy AA2195 at cryogenic temperatures, Mater. Des. 58 (2014) 445–450.
[32] W. Pachla, M. Kulczyk, J. Smalc-Koziorowska, M. Wróblewska, J. Skiba, S. Przybysz, M. Przybysz, Mechanical properties and microstructure of ultrafine grained commercial purity aluminium prepared by cryo-hydrostatic extrusion, Mater. Sci. Eng. A 695 (2017) 178–192.
[33] S.X. Li, G.R. Cui, Dependence of strength, elongation, and toughness on grain size in metallic structural materials, J. Appl. Phys. 101 (2007) 1–6.
[34] S. Kheiri, H. Mirzadeh, M. Naghizadeh, Tailoring the microstructure and mechanical properties of AISI 316L austenitic stainless steel via cold rolling and reversion annealing, Mater. Sci. Eng. A 759 (2019) 90–96.
[35] M. Razzaghi, H. Mirzadeh, M. Emamy, Unraveling the effects of Zn addition and hot extrusion process on the microstructure and mechanical properties of as-cast Mg–2Al magnesium alloy, Vacuum 167 (2019) 214–222.
[36] C.Y. Yu, P.W. Kao, C.P. Chang, Transition of tensile deformation behaviors in ultrafine-grained aluminium, Acta Mater. 53 (2005) 4019–4028.
[37] S.R. Casolco, M.L. Parra, G.T. Villaseñor, High strain rate superplasticity of a Zn-22 wt.%Al-x wt.%Ag alloys, J. Mater. Process. Technol. 174 (2006) 389–393.
[38] W. Bednarczyk, J. Kawałko, M. Wątroba, P. Bała, Achieving room temperature superplasticity in the Zn-0.5Cu alloy processed via equal channel angular pressing, Mater. Sci. Eng. A 723 (2018) 126–133.
[39] T.G. Langdon, Seventy-five years of superplasticity: historic developments and new opportunities, J. Mater. Sci. 44 (2009) 5998–6010.
[40] E. Goo, K.T. Park, Application of the von mises criterion to deformation twinning, Scripta Metall. Mater. 23 (7) (1989) 1053–1056.
[41] G. Mani, M.D. Feldman, D. Patel, C.M. Agrawal, Coronary stents: a materials perspective, Biomaterials 28 (2007) 1689–1710.
[42] P.K. Bowen, J. Drelich, J. Goldman, Zinc exhibits ideal physiological corrosion behavior for bioabsorbable stents, Adv. Mater. 25 (18) (2013) 2577–2582.
[43] A. Jarzębska, Synergistic Effect of Magnesium Addition and Hydrostatic Extrusion on Microstructure and Properties of Biodegradable Zinc-Based Material, Ph.D. Thesis, Institute of Metallurgy and Materials Science of Polish Academy of Sciences, 2019.
[44] B. Srinivasarao, A.P. Zhilyaev, T.G. Langdon, M.T. Perez-Prado, On the relation between the microstructure and the mechanical behavior of pure Zn processed by high pressure torsion, Mater. Sci. Eng. A 562 (2013) 196–202.
[45] W. Pachla, M. Kulczyk, M. Sus-Ryszkowska, A. Mazur, K.J. Kurzydlowski, Nanocrystalline titanium produced by hydrostatic extrusion, J. Mater. Process. Technol. (1–3) (2008) 173–182 205.
[46] W. Pachla, A. Mazur, J. Skiba, M. Kulczyk, S. Przybysz, Development of high-strength pure magnesium and wrought magnesium alloys AZ31, AZ61, and AZ91 processed by hydrostatic extrusion with back pressure, Int. J. Mater. Res. 103 (5) (2012) 580–589.
[47] M.A. Meyers, A. Mishra, D.J. Benson, Mechanical properties of nanocrystalline materials, Prog. Mater. Sci. 51 (2006) 427–556.
[48] H. Gong, K. Wang, R. Strich, J.G. Zhou, In vitro biodegradation behavior, mechanical properties, and cytotoxicity of biodegradable Zn–Mg alloy, J. Biomed. Mater. Res. B Appl. Biomater. 103 (8) (2015) 1632–1640.
[49] X. Liu, J. Sun, K. Qiu, Y. Yang, Z. Pu, L. Li, Y. Zheng, Effects of alloying elements (Ca and Sr) on microstructure, mechanical property and *in vitro* corrosion behavior of biodegradable Zn-1.5Mg alloy, J. Alloys Compd. 664 (2016) 444–452.